8. Formulation, development and evaluation of CS encapsulated poly-ε-caprolactone-chitosan based core-shell polymeric nanoparticles (CS-PCCSNs)

8.1 Experimental methods

8.1.1 Pre-formulation studies

The following preformulation studies were performed for successful development of CS-PCCSNs.

8.1.1.1 Drug excipients compatibility studies

8.1.1.1.1 Fourier transform infrared (FTIR) spectroscopy

FTIR spectroscopic study of CS, poly-ε-caprolactone (PCL), chitosan, poloxamer 188 and their physical mixture was conducted using FTIR spectrophotometer (Shimadzu, Model-8400S, Japan) in order to assess the possibility of chemical interaction, if any, between CS and other excipients. The analysis was performed by following the same protocol as mentioned in ***sub-section 5.1.1.2.1.***

8.1.1.1.2 Differential scanning calorimetry (DSC) study

The thermal behaviour of CS, PCL, chitosan, poloxamer 188 and their physical mixture was characterized by using TGA/DSC-1, Star® system (Mettler Toledo, Switzerland) with an auto cool accessory, for evaluating the compatibility of CS with other excipients. The analysis was performed by following the same protocol as mentioned in ***sub-section 5.1.1.2.2.***

8.1.2 Formulation of CS encapsulated poly-ε-caprolactone-chitosan based core-shell polymeric nanoparticles

PCL-chitosan based CS-PCCSNs were engineered by using nano-coprecipitation method with little modifications as earlier reported by Liu *et al* [251]. In brief,

accurately weighed amount of PCL and chitosan were co-dissolved in 5 ml of 90 %v/v acetic acid solution and allowed to stirr to form homogeneous mixture. The formed polymeric solution was injected dropwise into magnetically stirred 30 ml of aqueous solution containing CS (25 mg) and poloxamer 188 at room temperature. The resultant mixture was allowed to stirr for 6 hr on magnetic stirrer at 1500 rpm, in order to solidify and to form core-shell CS-PCCSNs. Subsequently, CS-PCCSNs were concentrated by removing organic phase using rotatory evaporator (IKA® RV10, Germany) under reduce pressure by blowing nitrogen. The resulting CS-PCCSNs were recovered by centrifugation at 15,000 rpm using cooling centrifuge (RC 4100 F, Eltek, Mumbai, India) for 15 min at 4 ^{o}C temperature. The supernatant was separated and kept aside for drug content analysis as described later. The nanoparticles were washed thrice and resuspended in a fixed volume of DDW. The CS-PCCNs were lyophilized with mannitol (2 %w/v) using freeze dryer (Labconco, USA) for 48 hr, at -45 ^{o}C and 0.050 mbar vacuum pressure. The lyophilized CS-PCCSNs were stored in a desiccator at 4 ^{o}C and reconstituted to their original volume with DDW by manual shaking prior to further use.

8.1.3 Experimental Design

8.1.3.1 Preliminary screening of variables by using Plackett-Burman screening design

A set of experiments with Plackett–Burman statistical experimental design was performed to screen the effect of various formulation and process variables on the CQAs of CS-PCCSNs [54, 177], as described in ***sub-section 5.1.3.1***. The Design Expert® software (Version 8.0.6.1, Stat-Ease Inc., Minneapolis, USA) was utilized for the generation of randomized design matrix and evaluation of statistical experimental

design. Each variable was represented at two levels, namely, "high" and "low". These levels define the upper and lower limits of the range covered by each variable. The level selection of different variables was based on a preliminary study and scientific findings in the literature. Different 11 independent variables were tested using 12 experimental runs. The selected experimental variables along with their levels, used for the screening design are depicted in Table 8.1.

Table 8.1. Experimental variables with their levels in Plackett-Burman screening design.

Variables	Level	
Independent Variables	Low (-1)	High (+1)
A : Concentration of PCL (%w/v)	0.2	0.5
B : Stirring speed (rpm)	1000	1500
C : Concentration of surfactant (%w/v)	0.5	1.5
D : Amount of drug (mg)	25	50
E : Organic phase/aqueous phase ratio (v/v)	0.17	0.33
F : Types of drug	CS	GAN
G : Concentration of chitosan (%w/v)	0.1	0.3
H : Stirring temp (^oC)	25	40
I : Stirring time (hr)	1	2
J : Dropping height (cm)	5	10
K : Dropping speed (ml/min)	1	2

Where, CS: Cromolyn sodium; GAN: Ganciclovir

The particle size (Y_1), EE (Y_2) and PDI (Y_3) of CS-PCCSNs were selected as dependent variables (CQAs). Results of the different experimental runs were analyzed by employing multiple linear regressions using one-way ANOVA, in order to determine the significance of the selected model along with the factor coefficients [54,

178]. Results obtained were statistically analyzed at 5% level of significance. All experiments were performed in a triplicate and randomized order.

8.1.3.2 Optimization of variables by using Box-Behnken Experimental Design

The critical variables obtained after preliminary screening through the Plackett-Burman screening design, were applied to RSM for statistical optimization of the CS-PCCSNs. In current study, a response surface method, 3-level, 4-factor, Box-Behnken experimental design with statistical model incorporating interactive and polynomial terms was utilised for optimization, quantification and establishing the relationship between the clusters of controlled independent variables and the physicochemical properties of CS-PCCSNs [179-181], as described in ***sub-section*** 5***.1.3.2***.

Based on initial screening in the preliminary studies, concentration of PCL (X_1), concentration of chitosan (X_2) and concentration of surfactant (X_3) were opted as four critical independent variables. Each critically selected variable is varied at three different levels. Higher, middle and lower level of each variable is coded as +1, 0 and -1, respectively, which were determined from preliminary experimentation. Other variables, which were evaluated in the preliminary Plackett-Burman screening design, were adjusted to the fixed level in the Box-Behnken experimental design owing to their statistically insignificant effects on the dependent variables. The studied particle size (Y_1), EE (Y_2) and PDI (Y_3) of prepared CS-PCCSNs were taken as dependent variables. All independent and dependent variables along with applied constraints, in the form of actual and coded levels are summarized in Table 8.2. The design matrix comprising of 17 runs, along with quadratic response surface and second order polynomial model was constructed by using Design-Expert software® (8.0.6.1, Stat-Ease Inc., Minneapolis, USA). All experiments were run in a randomized order to

avoid any possible source of experimental bias and to increase the predictability of the model [23].

Multiple linear regression was applied by employing the ANOVA, in order to ascertain the influence and significance of factors along with their interactive effect on the response variables. Numerical output of ANOVA was represented in terms of *p*-value and $p<0.05$ was considered as statistically significant. 3D response surface plots and second order polynomial models were generated to quantify the correlation between independent variables and dependent variables as well as to determine the design space [179-182].

Table 8.2. Independent variables with their levels and dependent variables in Box-Behnken experimental design

Independent variables	Coded levels of variables		
	Low	Medium	High
	-1	0	1
X_1 = Concentration of PCL (%w/v)	0.2	0.4	0.6
X_2 = Concentration of chitosan (%w/v)	0.1	0.2	0.3
X_3 = Concentration of surfactant (%w/v)	0.5	1	1.5
Dependent variables (Responses)	**Constraints**		
Y_1= Particle size (nm)	Minimize		
Y_2= Encapsulation efficiency (%)	Maximize		
Y_3= Polydispersity index (PDI)	Minimize		

After generating the polynomial equations for the respective dependent variables, desirability approach based numerical optimization technique was probed for optimizing the CS-PCCSNs with desired quality traits. The different constraints for independent variables were set in order to obtain the levels of independent variables, which would yield optimized CS-PCCSNs with maximum EE and minimum particle

size with low PDI. Desirability function was probed for combining all the responses in one measurement in order to predict the optimum levels for the independent variables. By considering this fact, the optimization was performed through the software for obtaining the best preferable formulation. Subsequently, the experimentally optimized formulation was prepared and tested to verify the correlation between the actual and predicted responses and thereby, validity of the model [23, 45, 179, 183]. The optimized CS-PCCSNs were further subjected to various characterizations, *in-vitro* and *in-vivo* evaluation studies.

8.1.4 Characterizations of CS-PCCSNs

8.1.4.1 Particle size, polydispersity index (PDI) and zeta potential

Measurement of particle size, zeta potential and PDI of prepared CS-PCCSNs was carried out by photon correlation spectroscopy using DELSA^{TM} NANO C particle size analyzer (Beckman Coulter, Inc., UK) at 25 ^{o}C temperature. The electrophoretic mobility of CS-PCCSNs, under the influence of an applied electric field was measured for determination of zeta potential [184, 185]. Analysis was performed by following the same protocol as described in ***sub-section 5.1.4.1.***

8.1.4.2. Encapsulation efficiency (EE) and drug loading

The EE (%) and drug loading (%) of CS in prepared CS-PCCSNs were determined spectrophotometrically (Shimadzu UV 1800, Japan) at λ_{max} of 239 nm by measuring the free amount of CS (un-entrapped) in supernatant obtained after the centrifugation (indirect method) [29, 45]. Analysis was performed by following the same protocol as described in ***sub-section 5.1.4.2.***

8.1.4.3 Solid state characterizations

8.1.4.3.1 Fourier transform infrared spectroscopy (FTIR) study

The FTIR spectra of CS, PCL, chitosan, poloxamer 188 and optimized CS-PCCSNs were recorded by following the same protocol and same instrument as mentioned in the ***sub-section 5.1.1.2.1*** in order to evaluate any significant change, if occurs, during the encapsulation of CS inside the matrix of poly-ε-caprolactone-chitosan based core-shell polymeric nanoparticles (PCCSNs).

8.1.4.3.2 Differential scanning calorimetry (DSC) study

The physical state of CS inside PCCSNs was assessed by DSC study. The DSC thermograms of CS, PCL, chitosan, poloxamer 188 and optimized CS-PCCSNs were recorded by following the same protocol and same instrument as mentioned in the ***sub-section 5.1.1.2.2***.

8.1.4.3.3 Powder X-ray diffractometry (PXRD) study

The PXRD patterns of pure CS, PCL, chitosan, poloxamer 188, physical mixture and optimized CS-PCCSNs were obtained by following the same protocol and same instrument as mentioned in the ***sub-section 5.1.4.3.3*** in order to determine the change in the physical state of CS, if occurs during the encapsulation process.

8.1.4.4 Shape and surface morphology

8.1.4.4.1 High resolution transmission electron microscopy (HR-TEM)

The shape and surface morphology of the optimized CS-PCCSNs was examined by following the same protocol and same instrument as mentioned in the ***sub-section 5.1.4.4.1.***

8.1.4.4.2 Atomic force microscopy (AFM)

The surface morphology of optimized CS-PCCSNs was visualized by following the same protocol and same instrument as mentioned in the ***sub-section 5.1.4.4.2.***

8.1.4.4.3 Confocal laser scanning microscopy (CLSM)

The core-shell structure of CS-PCCSNs was visualized by using confocal laser scanning microscope (LSM 510 META, Carl Zeiss Inc., USA). For this study, FITC tagged micron sized CS-PCCSNs were intentionally prepared by employing identical procedure. The only change was reduction in the stirring speed to 400 rpm [141]. The fluorescent shell was obtained by using the FITC tagged chitosan.

8.1.4.5 *In-vitro* drug release study

The *in-vitro* drug release study of optimized CS-PCCSNs was performed using modified dialysis bag diffusion technique in phosphate buffer pH 7.4. The same protocol was followed for *in-vitro* drug release study and release kinetic modeling as mentioned in the ***sub-section 5.1.4.5.***

8.1.4.6 Accelerated and real time storage stability study

The stability of optimized CS-PCCSNs was assessed over a period of 6 month at room temperature (25 $\pm$ 2 ^{o}C), refrigerated condition (4 $\pm$ 1 ^{o}C), and accelerated condition (40 $\pm$ 2 ^{o}C/75 $\pm$ 5 % RH) as per ICH guideline by following the same protocol as mentioned in the ***sub-section 5.1.4.6.***

8.1.4.7 Animal studies

8.1.4.7.1 Animals

The animal study protocol was duly approved by Central Animal Ethical Committee of Banaras Hindu University (No. Dean/2014/CAEC/856). The animal details are discussed earlier in ***sub-section 5.1.4.7.1.***

8.1.4.7.2 *Ex-vivo* intestinal permeation study

The intestinal permeation potential of CS-PCCSNs across the GIT was assessed by *ex-vivo* intestinal permeation study using non-everted gut sac technique. The same method was followed as described in **s*ub-section 5.1.4.7.2.***

8.1.4.7.3 *In-vivo* intestinal uptake study

The intestinal particulate uptake and permeation of CS-PCCSNs was visualized by CLSM upon oral administration of FITC tagged CS-PCCSNs in rats. *In-vivo* intestinal uptake study was performed by following the same method as described in ***sub-section 5.1.4.7.3.***

8.1.4.7.4 *In-vivo* pharmacokinetic study

8.1.4.7.4.1 *Dosing and sampling*

The same dosing and sampling protocol as described in ***sub-section 5.1.4.7.4.1*** was followed for the determination of pharmacokinetic profile of CS-PCCSNs after oral administration in the rats.

8.1.4.7.4.2 *Chromatography conditions and drug extraction*

The same in-house validated RP-HPLC method was followed for determination of CS concentration in blood plasma as described in ***sub-section 4.1.2*.** The details of

chromatography conditions and drug extraction are mentioned in ***sub-section 4.1.2.1 and 4.1.2.4***, respectively.

8.1.4.7.4.3 *Pharmacokinetic parameters*

Various pharmacokinetic parameters for CS-PCCSNs were determined as mentioned in ***sub-section 5.1.4.7.4.3*** using non-compartmental analysis of plasma drug concentration-time profile data through Winnonlin® 6.1 (Pharsight Corporation, Mountain View, CA) pharmacokinetic software.

8.1.4.7.5 *In-vivo* mast cell stabilizing activity

In-vivo mast cell stabilizing activity was studied by following the same protocol as mentioned in ***sub-section 5.1.4.7.5*** after oral administration of CS-PCCSNs in rats.

8.1.4.8 Statistical analysis

The similar statistical analysis was performed using the GraphPad Prism software (version 5.03, GraphPad Software, USA) as mentioned in ***sub-section 5.1.4.8.*** The *p*-value less than 0.05 was considered as statistically significant.

8.2 Results and discussions

8.2.1 Pre-formulation studies

8.2.1.1 Drug excipients compatibility studies

8.2.1.1.1 Fourier transform infrared (FTIR) spectroscopy

FTIR study was performed for evaluating the compatibility between CS and components of PCCSNs, which would be used for the preparation of CS-PCCSNs. The FTIR spectra of CS, PCL, chitosan, poloxamer 188 and their physical mixture are displayed in Figure 8.1. The FTIR spectra of CS (Figure 8.1 (a)) displayed the principle characteristic peaks of CS as C=O stretching (1640 cm^{-1}), asymmetric

COO^- stretching (1573 cm^{-1}), symmetric COO^- stretching (1410 cm^{-1}), broad O-H stretching (3416 cm^{-1}), C-H alkane stretching (2880 cm^{-1}) and aromatic C-H stretching (1477 cm^{-1}). Further, number of prominent absorption bands corresponding to vibration within the molecular structure, were detected in the fingerprint region (1400-600 cm^{-1}) [43, 45]. The FTIR spectra of PCL (Figure 8.1 (b)) exhibited asymmetric C-H stretching (2949 cm^{-1}) and C=O stretching (1727 cm^{-1}), whereas peak at 1293 cm^{-1} was indicative of C=O and C-C stretching in the crystalline phase [252].

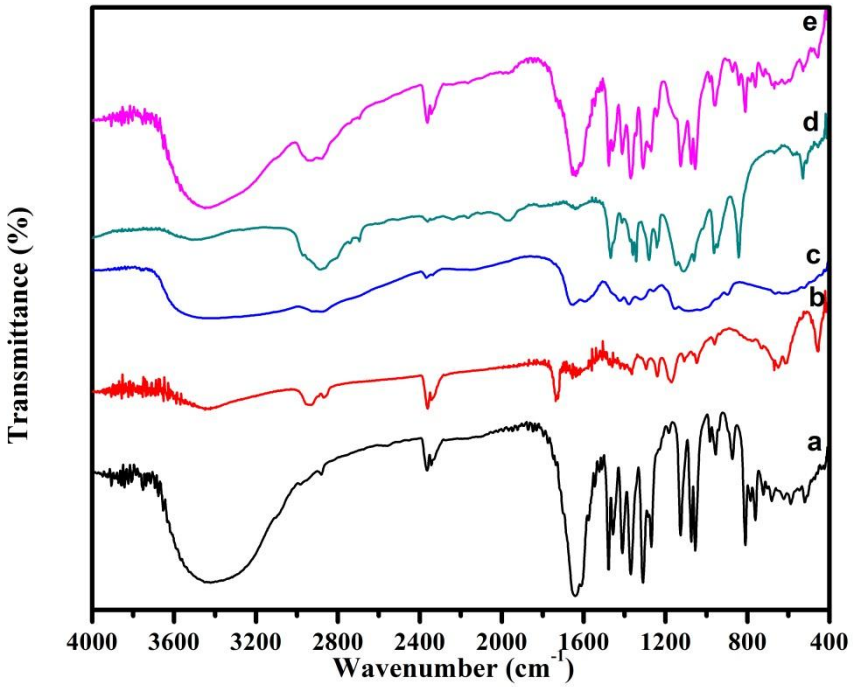

Figure 8.1 FTIR spectra of (a) CS, (b) PCL, (c) chitosan, (d) poloxamer 188 and (e) physical mixture

The characteristic peaks of chitosan were attributed at 3421 cm^{-1} (overlapped peaks of primary N-H_2 and O-H), 2922 cm^{-1} (C-H stretching), 1597 cm^{-1} (N-H bending), 1154 cm^{-1} (bridge-O-stretch) and 1654 cm^{-1} (C=O stretching of amide I) (Figure 8.1 (c)) [45, 253]. In case of FTIR spectra of poloxamer 188 (Figure 8.1 (d)), the

characteristic peaks were observed at wavenumber of 2882.41 cm^{-1} (C-H stretching) and 3400-3550 cm^{-1} (O-H stretching). All the major peaks pertaining to CS were clearly recognized in the FTIR spectra of physical mixture (Figure 8.1 (e)) at nearly same wavenumber as appeared in its pure spectra, suggesting the non-involvement of CS in any kind of physicochemical interaction with the other carrier excipients and existence of compatibility with the components of PCCSNs [40, 45].

8.2.1.1.2 Differential scanning calorimetry (DSC) study

DSC thermograms of CS, PCL, chitosan, poloxamer 188 and their physical mixture are depicted in Figure 8.2. In the DSC thermogram of pure CS (Figure 8.2 (a)), a sharp endotherm corresponding to its melting point was appeared at 264 ^{o}C, suggesting its intrinsic crystalline nature [45, 149]. PCL showed endothermic peak at 61 ^{o}C (Figure 8.2 (b)). No any sharp endotherm/exotherm related to degradation, phase transition or crystallinity was observed for chitosan, owing to its amorphous nature. Only broad hump was observed at around 90 ^{o}C due to its glass transition temperature (Figure 8.2 (c)) [45, 254]. Poloxamer 188 showed sharp endotherm at 55 ^{o}C corresponding to its melting point (Figure 8.2 (d)). In the thermogram of physical mixture of CS with the components of PCCSNs (Figure 8.2 (e)), a likewise thermal behaviour of CS and other components was noticed without any substantial shift in their endothermic peak positions, indicating absence of interaction of CS with other excipients. Additionally, no any new endothermic or degradation peak was observed in the thermogram of physical mixture (Figure 8.2 (e)), suggesting the existence of compatibility between CS and carrier components of PCCSNs [23, 45, 207].

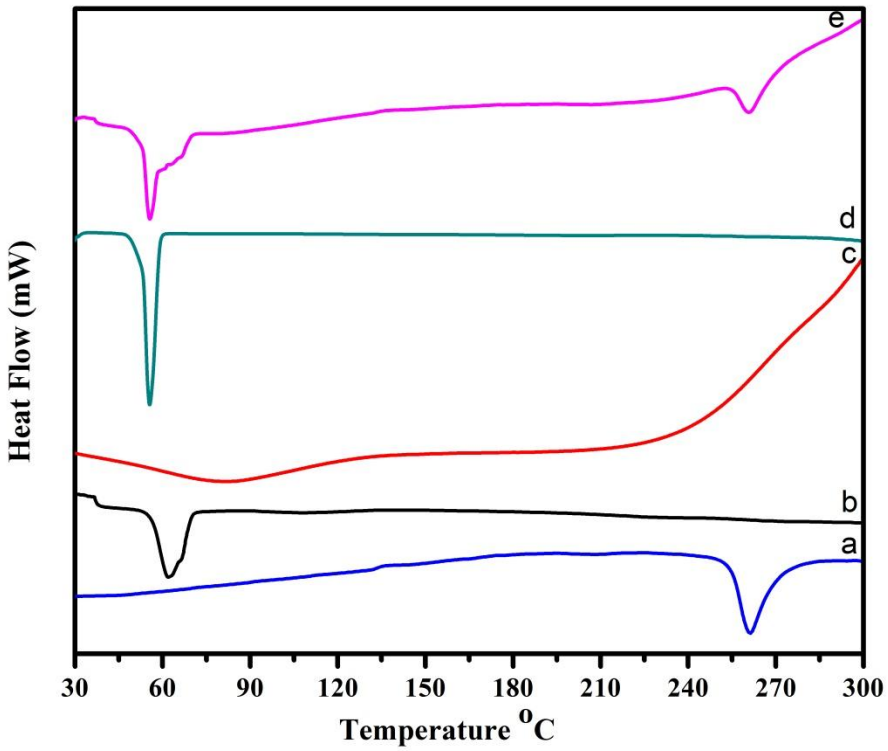

Figure 8.2 DSC thermograms of (a) CS, (b) PCL, (c) chitosan, (d) poloxamer 188 and (e) physical mixture

8.2.2 Experimental design

8.2.2.1 Preliminary screening of variables by using Plackett-Burman screening design

The physicochemical properties of CS-PCCSNs, prepared by modified nano-coprecipitation method are influenced by various formulation and process variables. The influence of various independent variables on the particle size, EE and PDI of the CS-PCCSNs (CQAs) were studied by 11-factor, 2-level Plackett-Burman screening design. The Plackett–Burman statistical experimental design was employed for the initial screening and selection of critical variables, affecting significantly to the formulation characteristics of CS-PCCSNs with good degree of accuracy, during

preliminary studies. It is a useful and efficient mathematical approach for evaluating the effect of large number of independent variables on particular CQAs, by performing relatively few numbers of experimental runs. Based on literature search and existing scientific knowledge, various independent variables were selected as they are likely to affects the physicochemical properties of CS-PCCSNs [54, 208, 209]. A total of 12 experimental trials, comprising of various combinations of different 11 independent variables were carried out as shown in Table 8.3.

Since, Plackett-Burman screening designs are resolution 4 designs, only main effects of the selected independent variables were analyzed. The wide variation was observed in the selected dependent variables of CS-PCCSNs, indicating that the independent variables had a significant effect on the response parameters chosen. Table 8.4 shows the results of different experimental runs in terms of different dependent variables.

Table 8.3 Plackett-Burman screening design experimental matrix.

Run	A	B	C	D	E	F	G	H	I	J	K
1	0.60	1000	1.50	50	0.17	GAN	0.30	40	1	5	1
2	0.60	1500	0.50	50	0.33	GAN	0.10	25	1	10	1
3	0.60	1500	1.50	25	0.17	CS	0.30	25	2	10	1
4	0.60	1000	0.50	25	0.33	CS	0.30	40	1	10	2
5	0.20	1000	1.50	25	0.33	GAN	0.10	40	2	10	1
6	0.20	1500	0.50	50	0.33	CS	0.30	40	2	5	1
7	0.20	1000	0.50	25	0.17	CS	0.10	25	1	5	1
8	0.60	1000	1.50	50	0.33	CS	0.10	25	2	5	2
9	0.20	1500	1.50	50	0.17	CS	0.10	40	1	10	2
10	0.60	1500	0.50	25	0.17	GAN	0.10	40	2	5	2
11	0.20	1000	0.50	50	0.17	GAN	0.30	25	2	10	2
12	0.20	1500	1.50	25	0.33	GAN	0.30	25	1	5	2

Where, CS: Cromolyn sodium; GAN: Ganciclovir

Table 8.4 Results of dependent variables obtained through Plackett-Burman design

Run	Particle Size (nm)	EE (%)	PDI
1	264.4 ± 3.8	67.3 ± 1.4	0.298 ± 0.056
2	266.7 ± 1.2	79.3 ± 0.7	0.378 ± 0.081
3	278 ± 4.3	83.4 ± 1.8	0.201 ± 0.046
4	329.6 ± 2.7	87.7 ± 2.3	0.271 ± 0.028
5	169.1 ± 2.9	59.2 ± 1.5	0.219 ± 0.034
6	243.1 ± 1.7	71 ± 0.4	0.399 ± 0.016
7	212.8 ± 1.1	55.4 ± 2.6	0.248 ± 0.072
8	234.4 ± 3.6	61.2 ± 1.7	0.223 ± 0.092
9	160 ± 2.8	66.1 ± 0.8	0.212 ± 0.037
10	261.3 ± 5.1	69.8 ± 0.3	0.192 ± 0.021
11	295.7 ± 4.2	85 ± 2.6	0.412 ± 0.034
12	178.1 ± 2.6	59 ± 1.4	0.181 ± 0.042

All values reported are mean ± SD; n = 3

Pareto chart showing the relative effect of the each independent variable on each dependent variable is depicted in Figure 8.3. It indicates the effect of independent variables plotted against the vertical axis as per their respective rank order. The variables for which, vertical bars extending passed the horizontal line suggested the statistical significance on the dependent variable [54, 210, 211].

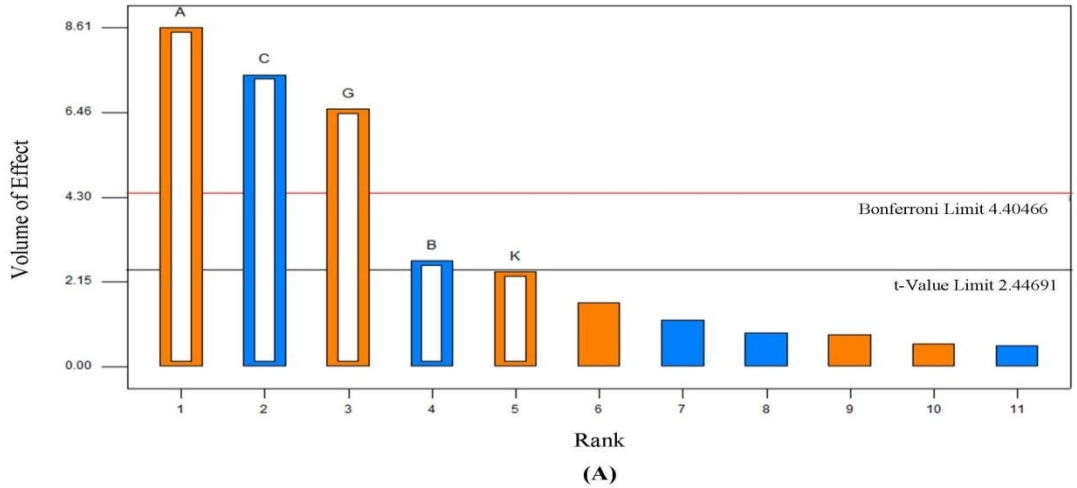

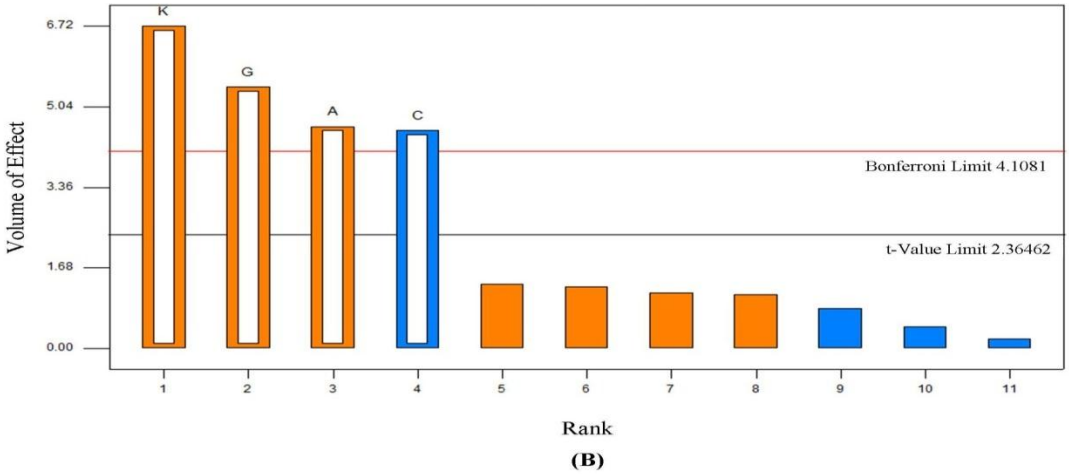

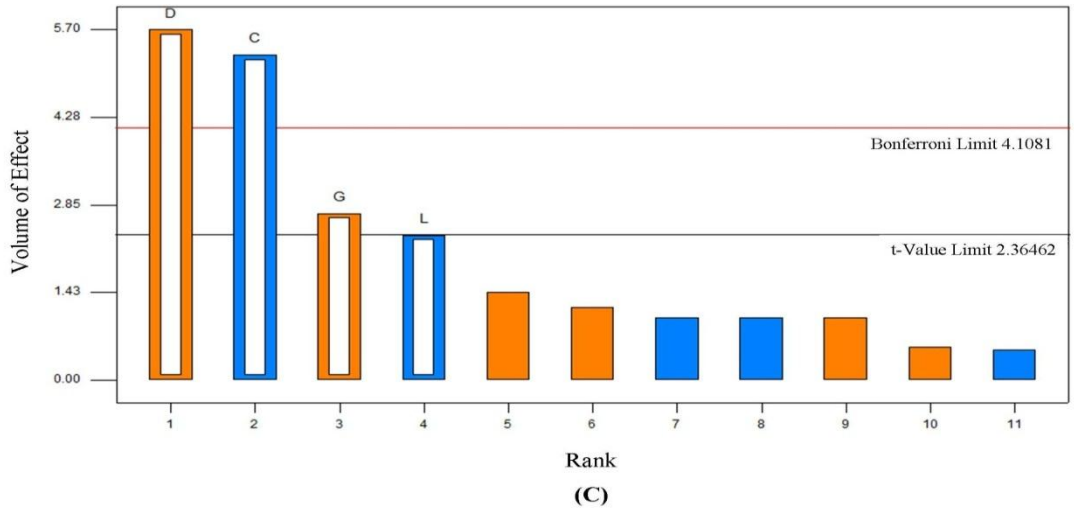

Figure 8.3 Pareto charts showing the significant effect of independent variables on (A) particle size, (B) EE and (C) PDI of CS-PCCSNs during Plackett-Burman screening design

Table 8.5 Statistical analysis of dependent variables of Plackett-Burman screening design

Factor	Y_1 = Particle size		Y_2 = EE		Y_3 = PDI	
	Coefficient	***p* Value**	**Coefficient**	***p* Value**	**Coefficient**	***p* Value**
A	31.25	0.0001	4.42	0.0024	-0.009	0.2547
B	-9.75	0.0363	1.07	0.1406	-0.009	0.1890
C	-26.92	0.0003	-4.33	0.0027	-0.047	0.0011
D	2.92	0.2824	1.28	0.1985	0.051	0.0007
E	-4.25	0.1710	-0.80	0.1380	0.009	0.2762
F	-1.92	0.1000	-0.43	0.2548	0.011	0.2231
G	23.75	0.0006	5.20	0.0010	0.024	0.0301
H	-3.08	0.2803	-0.18	0.1000	-0.004	0.1000
I	-5.92	0.1029	1.23	0.1843	0.004	0.4653
J	8.75	0.0526	6.42	0.0003	0.013	0.1697
K	2.08	0.4735	1.10	0.1947	-0.021	0.0506

Statistical analysis revealed that the particle size (Y_1) of the CS-PCCSNs was significantly ($p<0.05$) influenced by four independent variables, i.e., concentration of PCL (A), stirring speed (B), concentration of surfactant (C) and concentration of chitosan (G), as indicated in Figure 8.3 (A) and Table 8.5. The value of correlation coefficient (R^2) was found to be 0.9686, indicating the goodness of fit of the model being tested. The *p*-value for the regression model was found to be 0.0002 and was considered as significant. All other independent variables showed non-significant ($p>0.05$) impact on the particle size. The model fitting values for different dependent variables, which indicate model adequacy are listed in Table 8.6.

For EE (Y_2) of the CS-PCCSNs, the four most significant (p<0.05) independent variables were concentration of PCL (A), concentration of surfactant (C), concentration of chitosan (G) and dropping height (K) amongst all other independent variables selected, as depicted in Figure 8.3 (B) and Table 8.5. The R^2 value for the regression model was 0.9435, indicating the goodness of fit of the model being tested. The *p*-value for the regression model was found to be significant (p=0.0002), confirming the adequate fitting to the model. All other independent variables also affected EE, but their impact was statistically non-significant (p>0.05).

Table 8.6 Model summary statistics of the quadratic response surface models

Response Variable	Model						
	F-value	**Prob>F***	**R^2**	**Adj. R^2**	**Pred. R^2**	**Adeq. Prec.**	**C.V. (%)**
Y_1	36.97	0.0002	0.9686	0.9424	0.8742	20.614	5.22
Y_2	29.22	0.0002	0.9735	0.9112	0.8340	15.025	4.70
Y_3	18.37	0.0008	0.9130	0.8633	0.7444	12.262	11.45

*Adj. R^2: Adjusted R^2; Pred. R^2: Predicted R^2; Adeq. Prec.: Adequate Precision; C.V.: Coefficient of Variation; *Prob>F is the significance level and a value less than 0.05 considered significant.*

Whereas, PDI of the CS-PCCSNs was found to be most significantly (p<0.05) dependent on the concentration of surfactant (C), amount of drug (D) and concentration of chitosan (G) relative to other variables, as observed in Figure 8.3 (C) and Table 8.5. The R^2 value for the regression model was found to be 0.9130, suggesting the significant goodness of fit of the model. The significant *p*-value (p=0.0008) for the regression model confirmed the adequate fitting to the model. All other independent variables showed non-significant (p>0.05) impact on the PDI.

Thus, on the basis of results of the Plackett–Burman screening design, all the significantly affected independent variables on the physicochemical attributes of CS-PCCSNs were further evaluated by RSM for statistical optimization [54, 209, 210].

8.2.2.2 Formulation optimization of variables by using Box-Behnken experimental design

According to the results obtained from the Plackett-Burman screening design, the total of three independent variables, namely concentration of PCL, concentration of surfactant and concentration of chitosan were selected as critical variables for the statistical optimization of the CS-PCCSNs using RSM [23, 210]. As the particle size and EE are more important for oral delivery of nanoparticles based on scientific literature, all common three independent variables were considered for systemic optimization. Whereas, other independent variables, which have affected significantly on the single dependent variables, were fixed to their higher or lower level corresponding to their negative or positive effect, respectively. A 3-level, 3-factor Box-Behnken experimental design based RSM was performed for precisely exploring and optimizing the influence of three independent variables i.e. concentration of PCL (X_1), concentration of chitosan (X_2) and concentration of surfactant (X_3) on dependent variables, such as particle size (Y_1), EE (Y_2) and PDI (Y_3) of CS-PCCSNs. A total of 17 batches of CS-PCCSNs including 5 center points, were prepared as per design matrix generated by Box-Behnken experimental design by varying the four independent variables for all possible combinations. All the other independent variables used in the Plackett-Burman screening design, were found to have statistically non-significant effect on the physicochemical properties of CS-PCCSNs in the selected range and hence, set to fix level during optimization using RSM [209, 210]. The statistical treatment combinations of the different independent variables

along with the measured response variables, obtained by performing experiments are summarized in Table 8.7.

Regression models and polynomial equations explaining the main effect, interactive effect as well as quadratic effect of the various independent variables on dependent variables were generated by fitting the results of the experimental design, with the help of Design-Expert® software. Statistical significance of the selected model and the regression coefficients were estimated by multiple regressions using ANOVA. All the response variables were fitted to different regression models. For each response, the model which generated a higher F value was selected as the best fitted model. The accuracy and adequacy of the model was determined by measuring the R^2 value, which indicates the 'goodness of fit' of the model to the experimental results.

The positive coefficient in polynomial equation suggests that the response varies directly with successive increase in the value of independent variables (i.e., synergistic effect), whereas the negative sign indicates that the response decreases with successive increase the value of independent variables (i.e., inverse effect). The absolute value of the co-efficient indicates the magnitude of effect of the independent variables on the response variable; the higher the value the higher the magnitude [179, 211-213].

3D response surface plots were constructed using respective polynomial equations to reveal the interactive effect of any two independent variables on dependent variable graphically, keeping third one at a constant level. The relationships between the dependent variable and the independent variables were also visualized by 2D contour plots for understanding the relative influence of the independent variable along with in combinations [179, 180, 182]. The mathematical relationships of independent

variables' coefficients along with corresponding *p*-values for the dependent variables obtained by regression analysis are summarized in Table 8.8. *p*-value less than 0.05 was considered as statistically significance.

Table 8.7 Box-Behnken experimental design showing experimental runs with independent variables and their measured responses: particle size (Y_1), encapsulation efficiency (Y_2), and PDI (Y_3) of CS-PCCSNs.

Run No.	Independent variables			Dependent variables		
	X_1	X_2	X_3	Y_1	Y_2	Y_3
Factorial Points						
1	-1	-1	0	162.7 ± 7.1	70.1 ± 2.4	0.101 ± 0.018
2	1	-1	0	217 ± 2.6	80.6 ± 1.2	0.211 ± 0.024
3	-1	1	0	172 ± 3.1	74.1 ± 1.7	0.136 ± 0.017
4	1	1	0	266.2 ± 2.3	89.4 ± 1.1	0.378 ± 0.049
5	-1	0	-1	185.4 ± 5.7	76.2 ± 0.7	0.156 ± 0.081
6	1	0	-1	273 ± 11.3	89.5 ± 1.3	0.421 ± 0.076
7	-1	0	1	160.1 ± 8.4	69.4 ± 1.8	0.096 ± 0.034
8	1	0	1	227.4 ± 7.9	82.5 ± 2.1	0.231 ± 0.021
9	0	-1	-1	200.7 ± 6.3	77.3 ± 2.8	0.178 ± 0.064
10	0	1	-1	231 ± 5.2	83.1 ± 0.4	0.311 ± 0.038
11	0	-1	1	168.1 ± 4.3	72.8 ± 0.6	0.120 ± 0.042
12	0	1	1	202.9 ± 3.6	77.4 ± 0.9	0.189 ± 0.010
Centre Points						
13	0	0	0	230.5 ± 3.1	82.6 ± 1.2	0.287 ± 0.094
14	0	0	0	227.6 ± 2.3	84 ± 1.7	0.245 ± 0.046
15	0	0	0	236.2 ± 3.8	83.1 ± 0.9	0.331 ± 0.073
16	0	0	0	235.4 ± 4.7	83.4 ± 0.6	0.342 ± 0.038
17	0	0	0	229.3 ± 6.1	84.5 ± 1.4	0.276 ± 0.041

All data are shown as mean ± S.D; n=3

Table 8.8 Statistical analysis of dependent variables of Box-Behnken experimental design along with estimated regression coefficients and associated *p* values

Factor	Y_1 = Particle size		Y_2 = EE		Y_3 = PDI	
	Coefficient	*p* Value	Coefficient	*p* Value	Coefficient	*p* Value
Intercept	231.80	< 0.0001	83.52	< 0.0001	0.30	0.0007
X_1	37.92	< 0.0001	6.52	< 0.0001	0.092	< 0.0001
X_2	15.45	< 0.0001	2.90	< 0.0001	0.051	0.0031
X_3	-16.45	< 0.0001	-3.00	< 0.0001	-0.054	0.0022
X_1X_2	9.98	0.0006	1.20	0.0212	0.033	0.0807
X_1X_3	-5.07	0.0207	-0.050	0.9054	-0.033	0.0844
X_2X_3	1.12	0.5306	-0.30	0.4839	-0.016	0.3555
X_1^2	-8.26	0.0016	-1.61	0.0048	-0.032	0.0850
X_2^2	-19.06	<0.0001	-3.36	< 0.0001	-0.058	0.0078
X_3^2	-12.06	0.0002	-2.51	0.0004	-0.039	0.0442

8.2.2.2.1 Influence of Independent variables on particle size

The marked variation in the particle size of CS-PCCSNs, from minimum of 160.1 $\pm$ 2.5 nm to maximum of 273 $\pm$ 1.6 nm was observed for various experimental runs as per design matrix. The wide variation in the particle size indicates the substantial effect of selected formulation variables. The quadratic model was selected for the statistical analysis of influence of independent variables on particle size based on the lack of fit test as shown in Table 8.9.

Table 8.9 Statistical analysis results of lack of fit for particle size, EE and PDI of CS-PCCSNs

Source	Sum of Squares	df	Mean Square	F Value	p-value Prob > F	
Particle size						
Linear	3203.29	9	355.92	24.59	0.0037	-
2FI	2697.21	6	449.53	31.06	0.0026	-
Quadratic	23.57	3	7.86	0.54	0.6785	Suggested
Cubic	0.000	0	-	-	-	Aliased
Pure Error	57.90	4	14.47	-	-	-
Encapsulation efficiency						
Linear	102.41	9	11.38	20.43	0.0053	-
2FI	96.28	6	16.05	28.81	0.0030	-
Quadratic	2.39	3	0.80	1.43	0.3589	Suggested
Cubic	0.000	0	-	-	-	Aliased
Pure Error	2.23	4	0.56	-	-	-
PDI						
Linear	0.038	9	0.00420	2.62	0.1837	-
2FI	0.028	6	0.00470	2.93	0.1587	-
Quadratic	0.009005	3	0.00030	0.19	0.9002	Suggested
Cubic	0.000	0	-	-	-	Aliased
Pure Error	0.006423	4	0.00160	-	-	-

The empirical relationship between the particle size (Y_1) and independent variables, obtained after multiple linear regressions can be given by following second order polynomial equation (Eq (8.1)):

$$Y_1 = 231.80 + 37.92X_1 + 15.45X_2 - 16.45X_3 + 9.98X_1X_2 - 5.07X_1X_3 - 8.26X_1^2 - 19.06X_2^2 - 12.06X_3^2 \quad \text{Eq (8.1)}$$

Non-significant lack of fit value (p=0.6785; p>0.05) with F-value of 0.54 indicated that quadratic model is best fit to the independent variables for significantly describing the effect on the particle size. The high R^2 value (0.9957) implied the existence of reasonable agreement between predicted and experimental values for explaining the 99.57% variation in particle size. The minimal difference between predicted R^2 (0.9752) and adjusted R^2 (0.9901) value suggested the adequacy of the selected model for the prediction of response. The value of adequate precision was found to be 41.983 (greater than 4 is desirable), suggesting an adequate signal to measure the signal independent of noise. Further, low value for coefficient of variation (1.60 %) indicated high degree of precision and reliability of the model. Hence, this selected quadratic model can be used to navigate the design space [23, 54, 179, 212].

Statistical analysis revealed that concentration PCL (X_1) and concentration of chitosan (X_2) affects positively, whereas concentration of surfactant (X_3) provides negative effect on particle size. Also higher coefficient value (37.92) of concentration of PCL (X_1) suggested that it had most significant effect on particle size followed by concentration of surfactant (X_3) and concentration of chitosan (X_2). While in case of the interaction effects between different independent variables, concentration of PCL and concentration of chitosan (X_1X_2) as well as concentration of PCL and concentration of surfactant (X_1X_3) had combined significant effect on particle size. It is visually discerned from 3D response surface plots and 2D contour plots as displayed Figure 8.4.

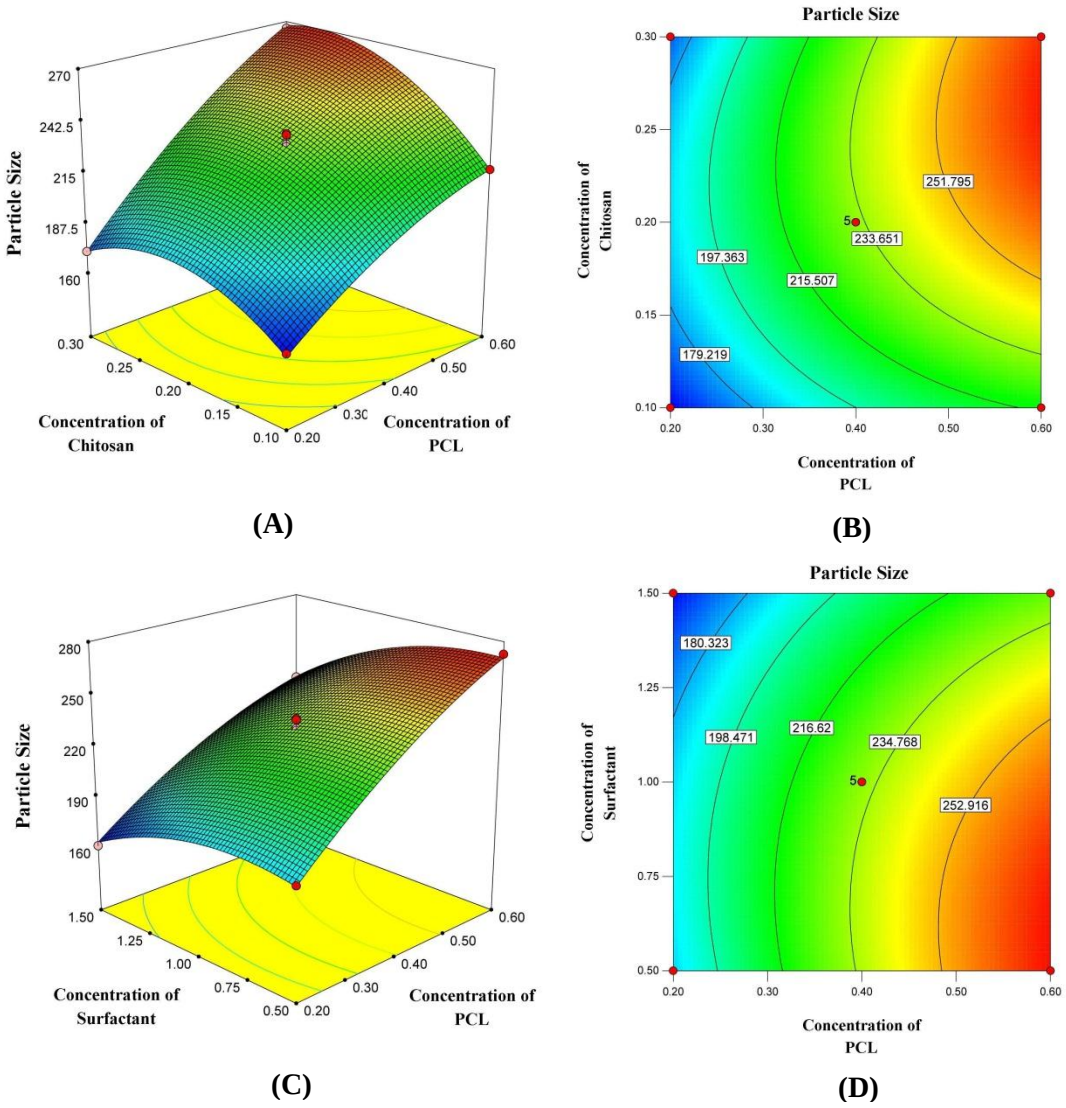

Figure 8.4 3D response surface plots (A), (C) and 2D contour plots (B), (D) showing the effect of independent variables (concentration of PCL, concentration of chitosan and concentration of surfactant) on particle size of CS-PCCSNs

The significant increase in particle size with an increase in concentration of PCL (X_1) might be resulted due to enhanced viscosity of dispersed phase as a consequence of triggering of polymer-polymer interactions. Higher viscosity would have reduced the shearing capacity of stirrer and have formed coarse dispersion with larger sized droplets. Moreover, the enhanced particle striking resulted from density difference between two phases, also might be the reason for generation of larger sized particles

[182, 214, 245]. Likewise behaviour was exhibited by the concentration of chitosan (X_2). This could be due to the fact that enhanced viscosity poses an obstacle to droplet breakdown by limiting the shearing stress of stirrer at the same input energy [45, 211, 255]. Nevertheless, concentration of surfactant (X_3) exhibited inverse relationship with particle size. The sharp decrease in particle size was observed at higher surfactant concentration might be due to sufficient surface coverage of the nanoparticles by surfactant molecules through interfacial localization, which would have imparted stabilization against particle impingement and thereby, prevented the formation of larger size particles [215, 245, 246].

8.2.2.2.2 Influence of Independent variables on encapsulation efficiency

For various factor level combinations, the EE of developed CS-PCCSNs was found to be varying in the range of 69.4 $\pm$ 0.7 % to 89.5 $\pm$ 2.6 %. The quadratic model was selected for the statistical analysis of influence of independent variables on EE of CS-PCCSNs, based on the lack of fit test as shown in Table 8.9. The second-order polynomial equation relating the EE (Y_2) and independent variables, generated by multiple linear regressions can be represented as follow in terms of coded variables (Eq (8.2)).

$$Y_2 = 83.52 + 6.52X_1 + 2.90X_2 - 3.00X_3 + 1.20X_1X_2 - 1.61X_1^2 - 3.36X_2^2 - 2.51X_3^2$$

Eq (8.2)

Non-significant lack of fit value (p=0.3589; p>0.05) with F-value of 1.43 indicated that quadratic model is best fit to the independent variables for significantly describing the influence on the EE. Good correlation between experimental and predicted values was noticed as revealed by R^2 value of 0.9921. The minimal difference between predicted R^2 (0.9288) and adjusted R^2 (0.9820) value indicated the

adequacy of the selected model for the prediction of response. The value of adequate precision was found to be 30.918 (greater than 4 is desirable), suggesting an adequate signal to measure the signal independent of noise. Further, low value for coefficient of variation (1.01 %) indicated high degree of precision and reliability of the model. Thus, all the above consideration indicated that the present quadratic model for EE can be used to navigate the design space [23, 54, 179, 212].

Statistical analysis revealed that concentration of PCL (X_1) and concentration of chitosan (X_2) affects positively, whereas concentration of surfactant (X_3) provides negative effect on EE of CS-PCCSNs. Also higher coefficient value (6.52) of concentration of PCL (X_1) suggested that it had most significant effect on EE followed by concentration of surfactant (X_3) and concentration of chitosan (X_2). While in case of the interaction effects between different independent variables, only concentration of PCL and concentration of chitosan (X_1X_2) had combined significant effect on EE. However, effect of independent variables on EE is lower than the effect on particle size. This is because of the lower coefficient value of the main effects and interaction terms in the polynomial equation of EE compared with the polynomial equation of particle size [54, 179]. 3D response surface plots and 2D contour plots portraying the effect of independent variables on EE of CS-PCCSNs are shown in Figure 8.5.

Amongst all, concentration of PCL (X_1) seems to be one of the most dominant variables, which positively influences the EE. The probable result might be the formation of viscous diffusional barrier on account of enhanced viscosity at higher concentration, which would have curtailed the drug diffusion [208, 216].

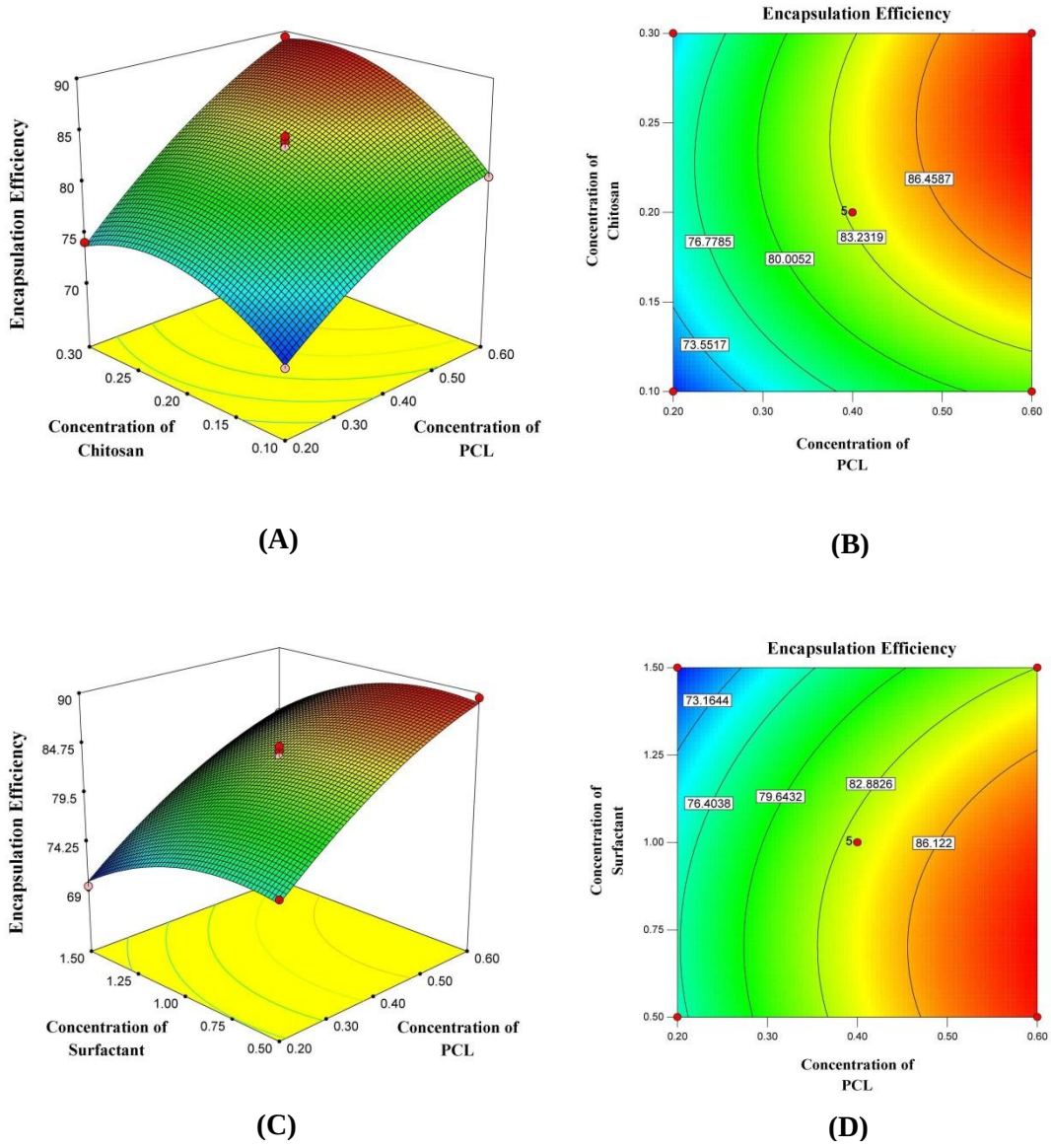

Figure 8.5 3D response surface plots (A), (C) and 2D contour plots (B), (D) showing the effect of independent variables (concentration of PCL, concentration of chitosan and concentration of surfactant) on encapsulation efficiency of CS-PCCSNs.

Likewise, concentration of chitosan (X_2) exhibited the enhanced EE at higher concentration, owing to their arrangement on the surface of polymeric nanoparticles to form core-shell architecture, which would have restricted the drug diffusion by imparting the barrier. Perhaps larger particle size obtained at higher concentration of PCL as well as chitosan also provided longer diffusional path, which might have

favored the high EE [45, 256]. Perversely, concentration of surfactant (X_3) affected negatively on the EE. This could be attributed to the reduced interfacial tension at higher surfactant concentration, which would have promoted the partition of drug into aqueous phase and contributed in substantive lowering of EE [208, 218].

8.2.2.2.3 Influence of independent variables on polydispersity index

The CS-PCCSNs exhibited relatively narrow particle size distribution varied from minimum of 0.096 $\pm$ 0.064 to maximum of 0.421 $\pm$ 0.089, as a consequence of varying the selected level combination of different independent variables. Low PDI values nearer to 0 indicate the relative homogenous nature of the dispersion. The quadratic model was selected for the statistical analysis of influence of independent variables on PDI of CS-PCCSNs, based on the lack of fit test as shown in Table 8.9. The following second order polynomial equation was obtained for describing the influence of independent variables on PDI (Y_3) in terms of coded variables (Eq (8.3)).

$$Y_3 = 0.30 + 0.094X_1 + 0.051X_2 - 0.054X_3 - 0.058X_2^2 - 0.039X_3^2 \qquad \text{Eq (8.3)}$$

The F-value of 0.19 with the absence of lack of fit value (p=0.9002; p>0.05) for quadratic model proves the excellent adequacy for significantly describing the influence of independent variables on the PDI. The higher R^2 value of 0.9538 suggests that 95.38% of variation in PDI was best explained by the formulation variables. The adequacy of the selected regression model for the prediction of response was supported by the minimal difference between predicted R^2 (0.8457) and adjusted R^2 (0.8944) value. The value of adequate precision was found to be 12.547 (greater than 4 is desirable), suggesting an adequate signal to measure the signal independent of noise. Further, low value for coefficient of variation (13.72 %) indicated high degree of precision and reliability of the model. Therefore, the

proposed quadratic model can be employed in order to navigate the design space [23, 54, 179, 212].

Statistical analysis revealed that concentration of PCL (X_1) and concentration of chitosan (X_2) affects positively, whereas concentration of surfactant (X_3) provides negative effect on PDI of CS-PCCSNs. Also higher coefficient value (0.094) of concentration of PCL (X_1) suggested that it had most significant effect on PDI followed by concentration of surfactant (X_3) and concentration of chitosan (X_2). Moreover, no any interactive effect of different independent variables on PDI was existed. However, effect of independent variables on PDI is lowest than the effect on particle size and EE. This is because of the lower coefficient value of the main effects and interaction terms in the polynomial equation of PDI compared with the polynomial equation of particle size and EE [54, 179]. 3D response surface plots and 2D contour plots portraying the effect of independent variables on PDI of CS-PCCSNs are depicted in Figure 8.6.

Significant growth in PDI value was noticed with successive increase in concentration of PCL (X_1) as well as concentration of chitosan (X_2). This might be ascribed to the fact that higher polymer concentration increases viscosity, which confines the shearing capacity of stirrer and forms coarse dispersion with different sized particles. Moreover, accelerated nucleation at higher polymer concentration and absence of sufficient surfactant molecule to stabilize the newly shaped particles also might have enforced the polydispersity [214, 219]. However, concentration of surfactant (X_3) showed contrary relationship with PDI. The monodisperesed CS-PCCSNs were formed at higher surfactant concentration as a result of marked reduction in the interfacial tension, as reported earlier [23, 54, 205].

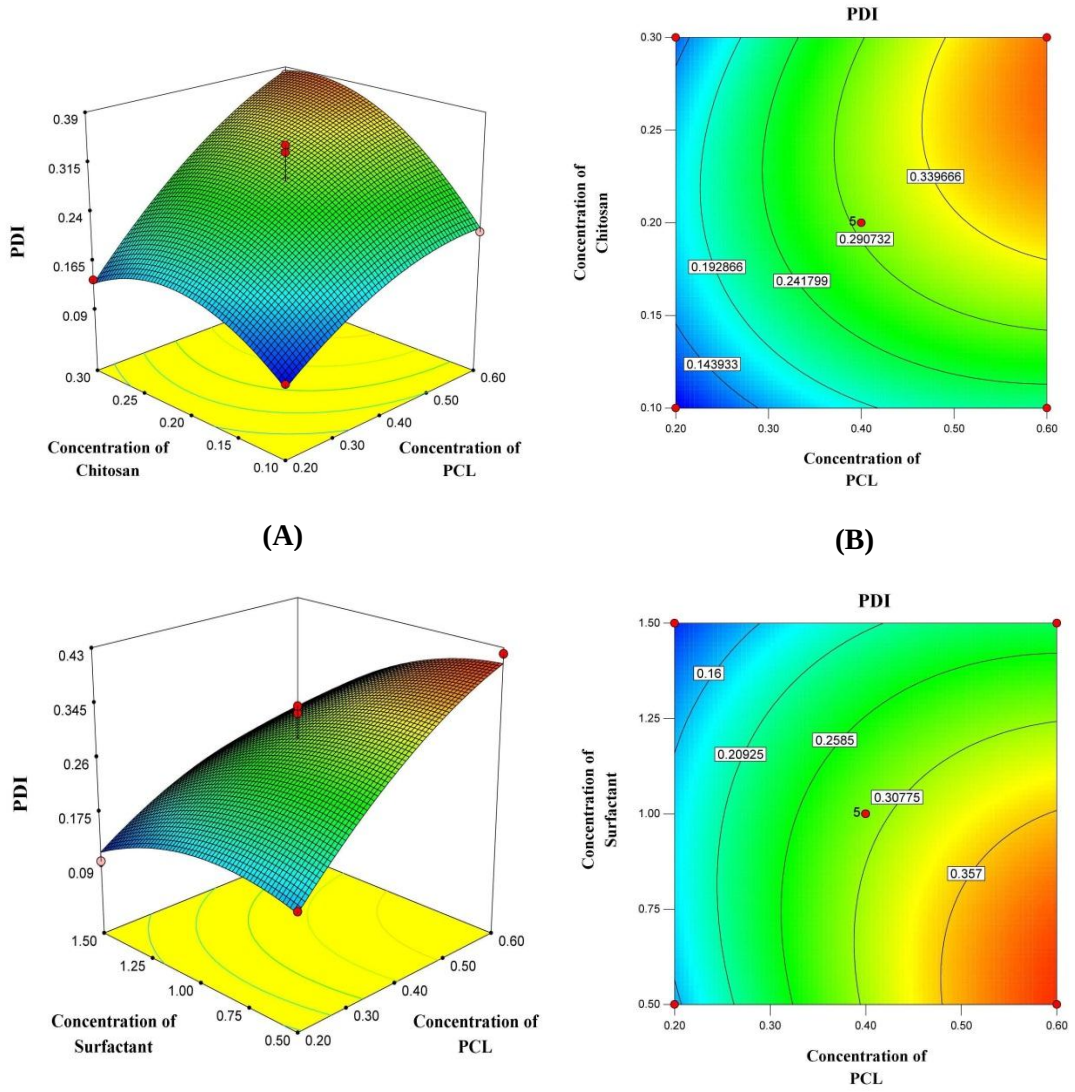

Figure 8.6 3D response surface plots (A), (C) and 2D contour plots (B), (D) showing the effect of independent variables (concentration of PCL, concentration of chitosan and concentration of surfactant) on PDI of CS-PCCSNs

8.2.2.2.4 Optimization of CS-PCCSNs using desirability function

Optimization of formulation by considering all the objectives at a time is difficult because of opposite effect of various independent variables. The optimum level of one independent variable might result in an inverse effect for other independent variable. Hence, the computer based numerical optimization with the aid of desirability function was probed for simultaneous optimization of the three independent variables

in order to produce optimized CS-PCCSNs having maximum EE without compromising with particle size and PDI. After setting the constraints during the optimization process, the levels of three different independent variables were determined using Design-Expert® software. The desirability of the optimized CS-PCCSNs was 0.628. The optimized CS-PCCSNs were formulated using predicted levels of respective independent variables for confirming the validity as well as predictive capability of experimental design as shown in Table 8.10.

Table 8.10 Comparison of experimental and predicted values of optimized CS-PCCSNs with its desirability generated by Design expert®

Independent variables	**Optimized levels**		
Concentration of PCL (X_1)	0.6 %w/v		
Concentration of chitosan (X_2)	0.11 % w/v		
Concentration of surfactant (X_3)	1.50 % w/v		
Results			
	Experimental values	**Predicted values**	**% Bias***
Particle size (nm)	194.2 ± 4.3	189.32	-2.57
Encapsulation efficiency (%)	77.34 ± 1.1	76.86	-0.62
Polydispersity index (PDI)	0.130 ± 0.026	0.128	-1.56
Overall Desirability	0.628		
Drug loading (%)	6.31 ± 0.43		
Zeta potential (mV)	(+) 18.4 ± 1.6		

**Bias was calculated as [(predicted value-experimental value)/predicted value] X 100;*

All results are shown as mean ±S.D; n=3

The close proximity with low percentage of bias between predicted results and experimental results reaffirmed the reliability of prognostic ability of Box Behnken experimental design for statistical optimization of desirable CS-PCCSNs, by considering all the objectives at a time. Optimized CS-PCCSNs were further selected for various *in-vitro* and *in-vivo* characterization studies. The useful results obtained by statistical analysis of data reiterated the utility of QbD approach in performing experiments [23, 179, 182, 183].

8.2.3 Characterizations of CS-PCCSNs

8.2.3.1 Solid state characterizations

8.2.3.1.1 Fourier transform infrared spectroscopy (FTIR) study

FTIR study was performed in order to evaluate chemical stability as well as to identify the significant change, if occurs during the encapsulation of CS inside the PCCSNs. The FTIR spectra of CS, PCL, chitosan, poloxamer 188 and optimized CS-PCCSNs are displayed in Figure 8.7. The FTIR spectra of CS (Figure 8.7 (a)) displayed the principle characteristic peaks of CS as C=O stretching (1640 cm^{-1}), asymmetric COO^- stretching (1573 cm^{-1}), symmetric COO^- stretching (1410 cm^{-1}), broad O-H stretching (3416 cm^{-1}), C-H alkane stretching (2880 cm^{-1}) and aromatic C-H stretching (1477 cm^{-1}). Further, number of prominent absorption bands corresponding to vibration within the molecular structure, were detected in the fingerprint region (1400-600 cm^{-1}) [43, 45]. The FTIR spectra of PCL (Figure 8.7 (b)) exhibited asymmetric C-H stretching (2949 cm^{-1}) and C=O stretching (1727 cm^{-1}), whereas peak at 1293 cm^{-1} was indicative of C=O and C-C stretching in the crystalline phase [252].

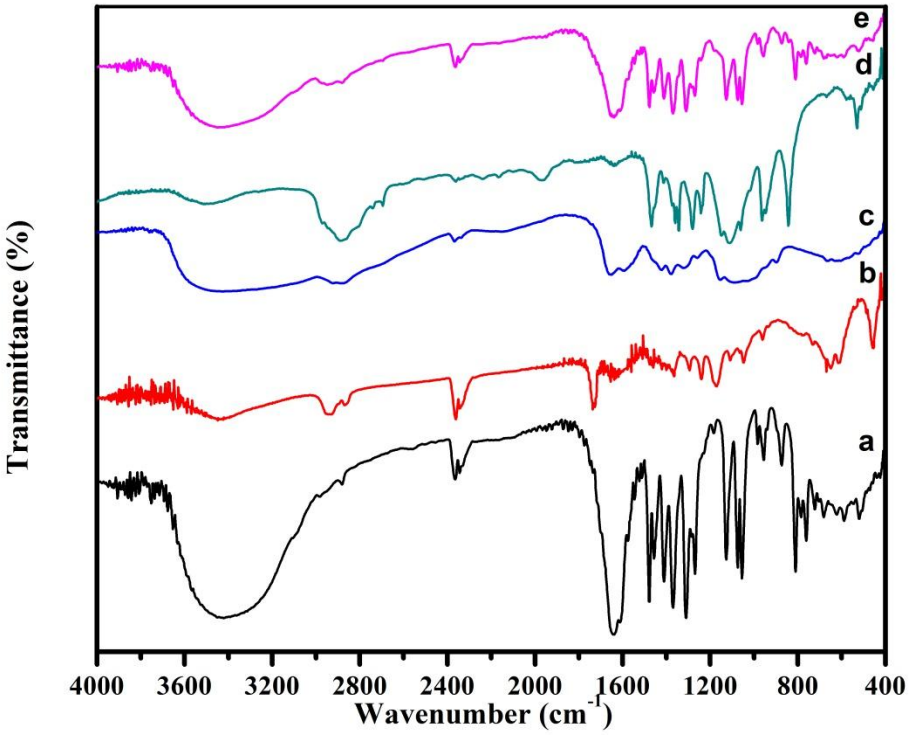

Figure 8.7 FTIR spectra of (a) CS, (b) PCL, (c) chitosan, (d) poloxamer 188 and (e) optimized CS-PCCSNs

The characteristic peaks of chitosan were attributed at 3421 cm^{-1} (overlapped peaks of primary N-H_2 and O-H), 2922 cm^{-1} (C-H stretching), 1597 cm^{-1} (N-H bending), 1154 cm^{-1} (bridge-O-stretch) and 1654 cm^{-1} (C=O stretching of amide I) (Figure 8.7 (c)) [45, 253]. In case of FTIR spectra of poloxamer 188 (Figure 8.7 (d)), the characteristic peaks were observed at wavenumber of 2882.41 cm^{-1} (C-H stretching) and 3400-3550 cm^{-1} (O-H stretching). Further, the position of the characteristic peaks of CS remain unaffected and appeared clearly in the spectra of optimized CS-PCCSNs (Figure 8.7 (e)) at nearly same wavenumber as appeared in its pure spectra, which proved successful encapsulation of CS inside the PCCSNs without any strong molecular alteration in its chemical nature during the encapsulation process [23, 49, 221].

8.2.3.1.2 Differential scanning calorimetry (DSC) study

DSC thermograms of CS, PCL, chitosan, poloxamer 188 and their physical mixture are depicted in Figure 8.8. In the DSC thermogram of pure CS (Figure 8.8 (a)), a sharp endotherm corresponding to its melting point was appeared at 264 ^{o}C, suggesting its intrinsic crystalline nature. Further, any peaks pertaining to release of absorbed moisture or nonstructural water as well as solid state transitions were not observed [45, 149, 210]. PCL exhibited sharp endothermic peak at 61 ^{o}C (Figure 8.8 (b)). No any sharp endotherm/exotherm related to degradation, phase transition or crystallinity was observed for chitosan, owing to its amorphous nature. Only broad hump was observed at around 90 ^{o}C due to its glass transition temperature (Figure 8.8 (c)) [45, 254]. Poloxamer 188 showed sharp endotherm at 55 ^{o}C corresponding to its melting point (Figure 8.8 (d)). Conversely, the crystalline to amorphous phase transformation of CS during the fabrication, was clearly identified in the thermogram of CS-PCCSNs (Figure 8.8 (e)) due to complete disappearance of endothermic peak at 264 ^{o}C. It also indicated that CS is dispersed as an amorphous molecular dispersion for inside the matrix of CS-PCCSNs. The probable reason might be the prevention of recrystallization of CS from the droplets due to high shear stress, which would have ultimately favored the homogeneous dispersion of CS as amorphous or disordered-crystalline drug phase, inside the CS-PCCSNs [188, 247]. This behaviour would be expected to improve the sustained release pattern without any burst effect, resulting in improved mean residence time in the body. The thermal behaviour of other excipients remained same as their pure thermograms. Furthermore, the absence of any new redundant endothermic peaks in the thermogram of CS-PCCSNs confirmed that the matrix of PCCSNs have homogeneously encapsulated the CS in an amorphous form during the encapsulation process, without any interactions [207, 210, 224].

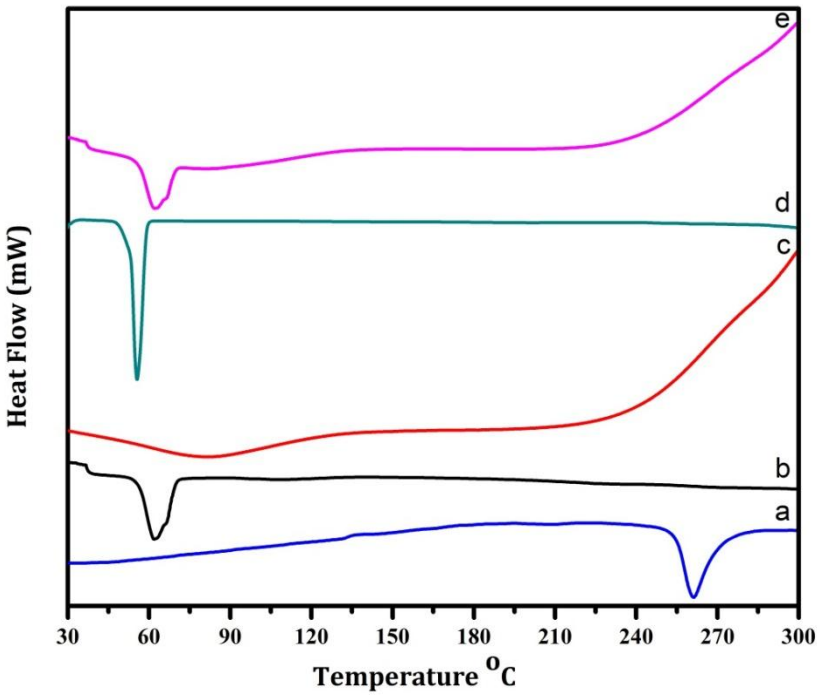

Figure 8.8 DSC thermograms of (a) CS, (b) PCL, (c) chitosan, (d) poloxamer 188 and (e) optimized CS-PCCSNs

8.2.3.1.3 Powder X-ray diffractometry (PXRD) study

Powder X-ray diffractogarms of pure CS, PCL, chitosan, poloxamer 188, their physical mixture and optimized CS-PCCSNs are depicted in Figure 8.9. The powder X-ray diffraction pattern of pure CS (Figure 8.9 (a)) exhibited that drug has crystalline nature with distinctive intense, sharp diffraction peaks observed at 2θ value of 8º, 9.83º, 11.5º, 14º, 16.9º, 19.7º, 24.3º, 26.6º and numerous minor peaks up to 35º [45, 149]. The diffraction patterns of the PCL (Figure 8.9 (b)) displayed two intense peaks at around 21.3º and 23.9º (2θ) along with hump shaped, abridged peaks due to scattering from the crystalline and amorphous regions, respectively [252]. Similarly, broad halo comprising of small diffuse peaks with two prominent high intensity peaks at 11º and 20º (2θ) were noticed for chitosan (Figure 8.9 (c)) [45]. The diffraction

patterns of Poloxamer 188 (Figure 8.9 (d)) also exhibited number of small diffuse peaks with two crystalline peaks.

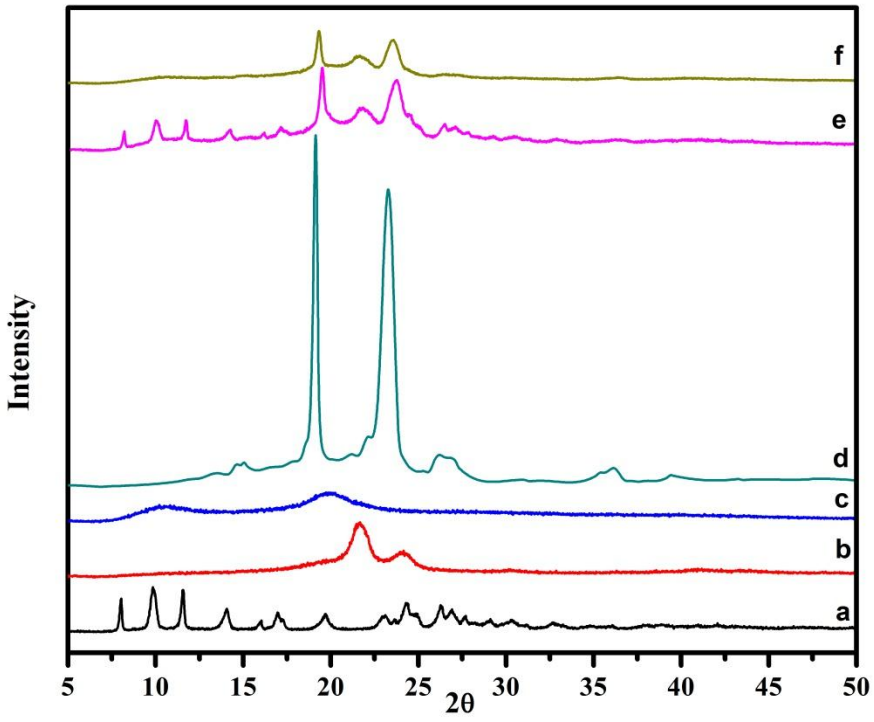

Figure 8.9 PXRD patterns of (a) CS, (b) PCL, (c) chitosan, (d) poloxamer 188, (e) physical mixture and (f) optimized CS-PCCSNs

Further, retention of crystallinity of CS without any interaction was detected in the diffractogram of physical mixture (Figure 8.9 (e)), as indicated by its sharp peaks, which were seemed at nearly same 2θ angles. Since PCL, chitosan and poloxamer 188 exhibited no any characteristic diffraction peaks up to 20°, the crystalline peaks must be originated from the crystalline region of CS due to absence of any interaction. However, PXRD pattern of CS-PCCSNs (Figure 8.9 (f)) suggested that the physical state morphosis of CS has taken place from crystalline to amorphous state upon encapsulation inside the matrix of PCCSNs, as indicated by its broad, diffuse and stifled diffraction peaks. Moreover, the peaks with abridged intensity also reflected

the destruction of the native chitosan packing structure. It might be due to recrystallization of chitosan, which would have resulted in the alteration of the arrangement of molecules in crystal lattice and would responsible for imparting stability to CS-PCCSNs [210, 226, 247]. PXRD results are in good agreement with the results demonstrated by DSC, confirming the homogeneous and complete encapsulation of CS inside the matrix of the PCCSNs [23, 224, 248].

8.2.3.2 Shape and surface morphology

8.2.3.2.1 High resolution transmission electron microscopy (HR-TEM)

The shape and surface morphology of the optimized CS-PCCSNs was examined by employing HR-TEM. The HR-TEM micrographs (Figure 8.10 (A)) exhibited nano-sized, uniform, discrete CS-PCCSNs with spherical morphology. The aggregation was not detected among unimodal, CS-PCCSNs possibly due to steric hindrance offered by charged surface. The external surface of CS-PCCSNs was smooth without any discernible, rough pores or crevices. Under high magnification, the striking core-shell architecture was observed for CS-PCCSNs, which have dark inner PCL containing core enveloped by very light chitosan shell. The probable reason behind the clear visualization of the distinct core-shell nanostructure could be the apparent electron density difference between two polymer compositions [23, 50].

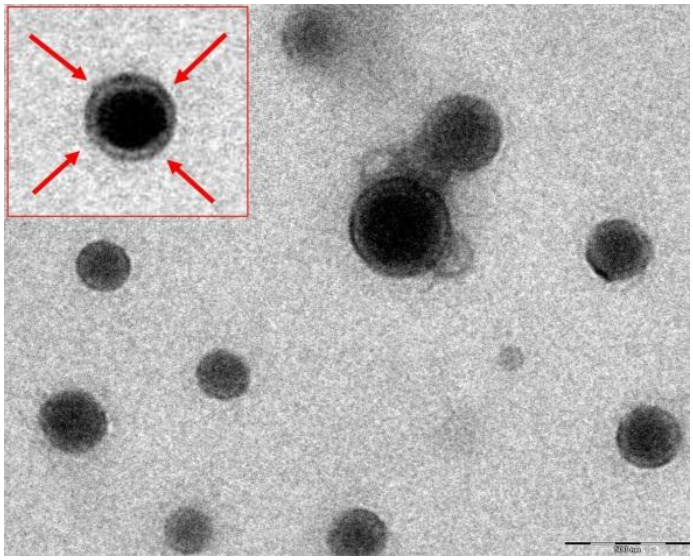

(A)

(B)

Figure 8.10 (A) HR-TEM image of optimized CS-PCCSNs, Inset image shows core-shell architecture of the CS-PCCSNs; (B) Electron diffraction pattern of optimized CS-PCCSNs

The particle size obtained with HR-TEM micrographs was comparable to that obtained by particle size analyzer using dynamic light scattering technique, in which most of them are smaller than 225 nm. Furthermore, the physical state of CS inside

the PCCSNs was confirmed by generating electron diffraction (ED) pattern through HR-TEM. The ED pattern of CS-PCCSNs (Figure 8.10 (B)) exhibited the smooth diffraction halo pattern with absence of bright spots, corresponding to drug crystals in the diffraction ring pattern. An amorphous ED halo confirmed the encapsulation of CS in an amorphous molecular dispersion form inside the PCCSNs [23, 198, 226], which strengthens the results inferred from solid state characterizations.

8.2.3.2.2 Atomic force microscopy (AFM)

The surface morphology of optimized CS-PCCSNs was further determined by AFM study in order to confirm the morphological aspect revealed by HR-TEM. The topographic and 3D AFM micrographs of CS-PCCSNs, generated by the atomic level interaction between a sharp probing tip and the surface of CS-PCCSNs with a spatial resolution up to 0.01 nm, are depicted in Figure 8.11 (A) & (B). AFM micrographs corroborated well with the morphological features displayed by HR-TEM images and showed spherical shaped CS-PCCSNs having smooth texture without any ruptures or crevices. The uniform self-assembling of chitosan envelop over the PCL nanoparticles might be accounted for the smooth surface, which has varnished the indentations, formed by the diffusion of organic solvent from polymer matrix, during fabrication process [23, 188]. A reasonable correlation was noticed for the particle size determined during dynamic light scattering technique and morphological studies. The geometric diameter of CS-PCCSNs, determined by AFM was under 225 nm.

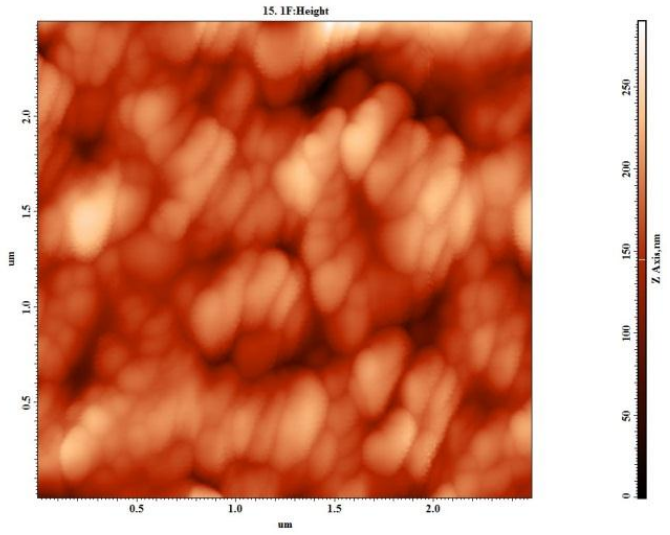

(A)

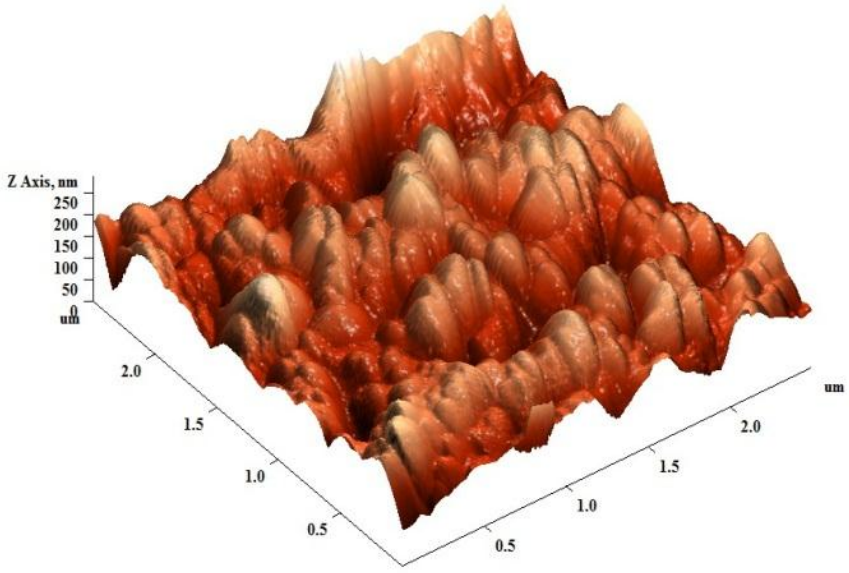

(B)

Figure 8.11 AFM images of optimized CS-PCCSNs (A) 2D micrograph and (B) corresponding 3D micrographs.

8.2.3.2.3 Confocal laser scanning microscopy (CLSM)

Additionally, confocal microscopy was used for confirming the core-shell nanostructure of the developed CS-PCCSNs. FITC labeled chitosan was used to

differentiate the core-shell architecture. The well distinguished two regions of different materials were observed in the CLSM micrograph (Figure 8.12 (A) & (B)), upon visualization under confocal microscope. CS-PCCSNs exhibited dark colored, hydrophobic PCL core enveloped by green colored, hydrophilic chitosan shell, which corroborates well with the findings of HR-TEM study [23, 141].

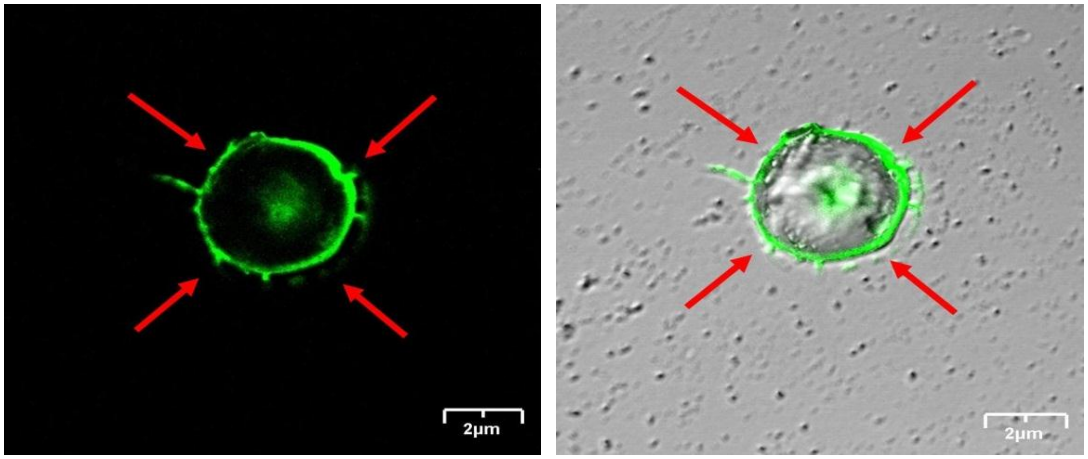

(A) **(B)**

Figure 8.12 (A) Fluorescent confocal microscopic image and (B) 3D - Confocal microscopic image of micron sized CS-PCCSNs tagged with FITC, showing core-shell architecture

8.2.3.3 *In-vitro* drug release study

In-vitro drug release study was performed in order to assess the potential of CS-PCCSNs to control the release of CS for prolonging the action. The CS release from CS-PCCSNs showed phasic release behaviour in phosphate buffer pH 7.4, comprising of initial burst release followed by extended release over a period of 48 hr as illustrated in Figure 8.13. The optimized CS-PCCSNs exhibited around 91% drug release at the end of 48 hr. The small initial burst comprising of nearly 14% drug, was observed within 1 hr (Table 8.11). This might be due to rapid diffusion of surface localized, weakly bound drug, which has easy access to solid/water interface.

Subsequently, an extended release was attained up to 48 hr, suggesting the slower immobilization of the uniformly encapsulated CS from polymer matrix on account of increased diffusion path and tortuosity [227]. This also might likely be due to core-shell architecture of the CS-PCCSNs, in which chitosan shield would has constrained the infiltration of water to the PCL matrix and thereby, decelerated the faster diffusion and controlled the release of CS [36, 248].

Table 8.11 *In-vitro* drug release data of the optimized CS-PCCSNs in phosphate buffer pH 7.4

Time (hr)	Cumulative % drug release
0	0
1	14.50 ± 0.62
2	18.85 ± 0.22
3	20.44 ± 0.50
4	24.84 ± 1.39
5	26.62 ± 1.69
6	28.93 ± 0.97
7	32.17 ± 1.69
8	34.95 ± 1.39
10	37.91 ± 2.00
12	42.73 ± 3.15
18	54.58 ± 5.00
24	63.47 ± 1.38
36	83.10 ± 3.21
48	91.80 ± 1.54

All values reported are mean ± SD, (n=3).

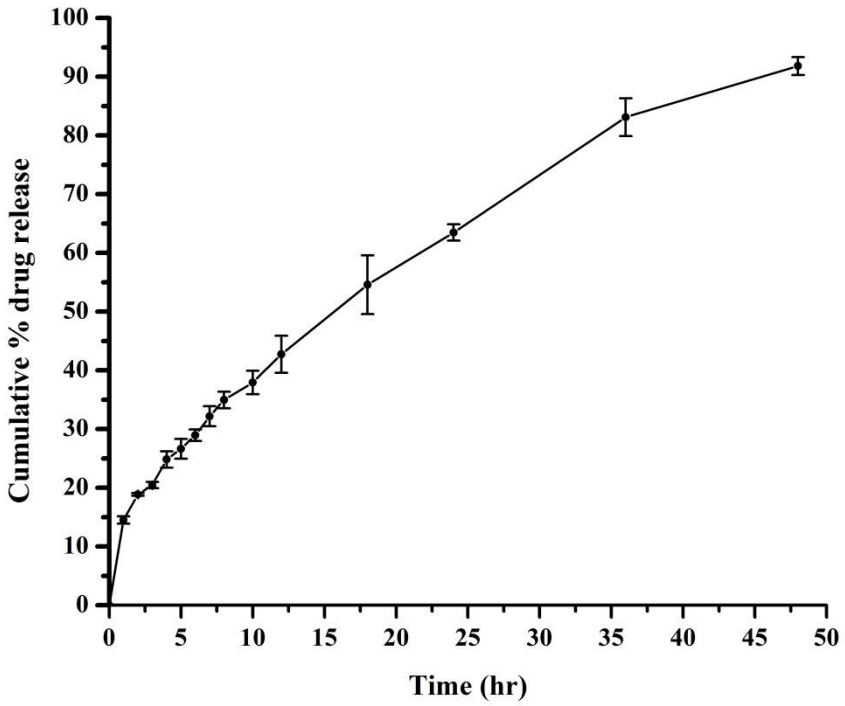

Figure 8.13 *In-vitro* drug release profile of optimized CS-PCCSNs in phosphate buffer pH 7.4 (vertical bar represents ± S.D; n=3)

Furthermore, the drug release mechanism and kinetics was determined by substituting the drug release profile data of CS-PCCSNs to different release kinetic models (i.e., zero order, first order, Higuchi model and Korsmeyer-Peppas model). The release kinetic modeling suggested that the drug release behaviour of CS from the CS-PCCSNs was best controlled by Fickian diffusion process as evident from Higuchi model (highest R^2 value compared to other kinetic models as shown in Table 8.12). Further, the release exponent (n) value obtained by fitting Korsmeyer-Peppas semi empirical model was found to be 0.499, which is suggestive that the drug release occurred through Fickian diffusion based controlled release pattern from the matrix of the CS-PCCSNs ($n<0.5$ for fickian diffusion) [191, 192]. It is speculated for CS like hydrophilic drug molecule to mobilize by diffusion mechanism as reported earlier

[243]. Hence, it is possible to achieve fluctuation free steady state CS plasma level upon oral administration of CS-PCCSNs, which provides loading dose as well as maintenance dose due to initial burst release followed by extended release [23, 49].

Table 8.12 Release kinetic models for simulation of release behaviour of CS from optimized CS-PCCSNs in phosphate buffer pH 7.4

Batch	Zero Order	First Order	Higuchi Model	Korsemeyer-Peppas model
Optimized CS-PCCSNs	$R^2 = 0.9689$ $K_z = 1.671$	$R^2 = 0.8397$ $K_F = 0.0361$	$R^2 = 0.9929$ $K_H = 13.571$	$R^2 = 0.9871$ $K_P = 12.658$ $n = 0.4996$

8.2.3.4 Accelerated and real time storage stability study

The ability of any colloidal system to remain stable against environmental changes is of prime requirement to ensure its final performance in terms of its *in-vivo* fate. Nanoparticles have very high tendency to agglomerate owing to their large surface-area-to-volume ratio, which results in the increase in particle size after longer periods of storage. The changes in the physical appearance, color, odor, taste, or texture of the formulation indicate the instability. The stability and intactness of CS-PCCSNs was assessed over a period of 6 month at room temperature (25 $\pm$ 2 ^{o}C), refrigerated condition (4 $\pm$ 1 ^{o}C), and accelerated condition (40 $\pm$ 2 ^{o}C/75 $\pm$ 5 % RH). The physical appearance and physicochemical attributes (i.e., particle size, EE and PDI) were chosen as stability indicating parameters. The changes in the physicochemical attributes of the CS-PCCSNs during the stability study over the period of 6 months are depicted in Figure 8.14.

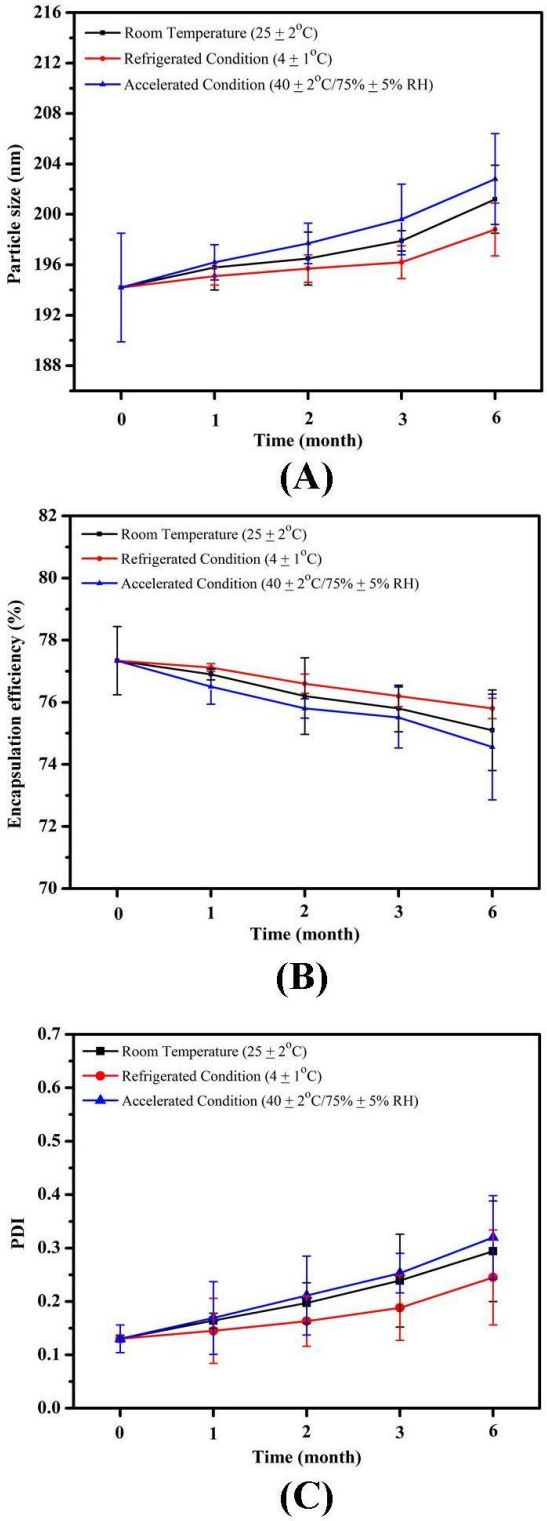

Figure 8.14 Effect on (A) particle size, (B) EE and (c) PDI of optimized CS-PCCSNs stored at different environmental conditions over different time interval (vertical bars represent ± SD; n=3)

The physical appearance of the CS-PCCSNs did not show any significant difference (i.e., lump formation and discoloration) at different environmental conditions during the study. Depositions formed on the base of container during storage were easily redispersible on mere shaking. Similarly, insignificant (p>0.05) change in the particle size, EE and PDI of CS-PCCSNs was observed during the storage at different environmental conditions, indicating the high stability of CS-PCCSNs to withstand the environmental fluctuations [45]. Hence, the stability study indicated that the developed CS-PCCSNs are physically as well as chemically stable and able to retain their pharmaceutical properties at various environmental conditions for safe and effective long-term use [49, 193, 228, 229].

8.2.3.5 *Ex-vivo* intestinal permeation study

The *ex-vivo* permeation study using non-everted rat intestinal model was accomplished in order to assess the permeation potential of CS-PCCSNs. The significant improvement in the intestinal permeation of CS, approximately ~8 folds (p<0.05) was observed by encapsulating inside PCCSNs as compared to CS solution. Figure 8.15 represents the intestinal permeation profile of CS from CS solution and CS-PCCSNs, along with their apparent permeability coefficient (Papp). The Papp value for CS from CS solution and CS-PCCSNs were found to be 0.909 ($\pm$ 0.049) × 10^{-5} cm/s and 7.781 ($\pm$ 0.413) × 10^{-5} cm/s, respectively. The poor permeation for CS solution was ascribed to its tween carboxylic acid group, which are responsible for imparting the high hydrophilicity [43, 45].

Table 8.13 *Ex-vivo* permeation data of the CS solution and optimized CS-PCCSNs across rat intestinal membrane

Time (min)	Cumulative % drug permeated	
	CS solution	CS-PCCSNs
0	0	0
15	1.21 ± 0.039	5.03 ± 0.46
30	2.40 ± 0.021	12.58 ± 1.25
45	3.33 ± 0.053	24.95 ± 1.84
60	4.39 ± 0.052	36.32 ± 2.28
90	4.98 ± 0.083	47.87 ± 1.89
120	5.71 ± 0.539	53.19 ± 1.64
180	6.78 ± 0.504	58.61 ± 2.42
240	7.71 ± 0.588	64.16 ± 3.88

All values reported are mean ± SD, (n=3)

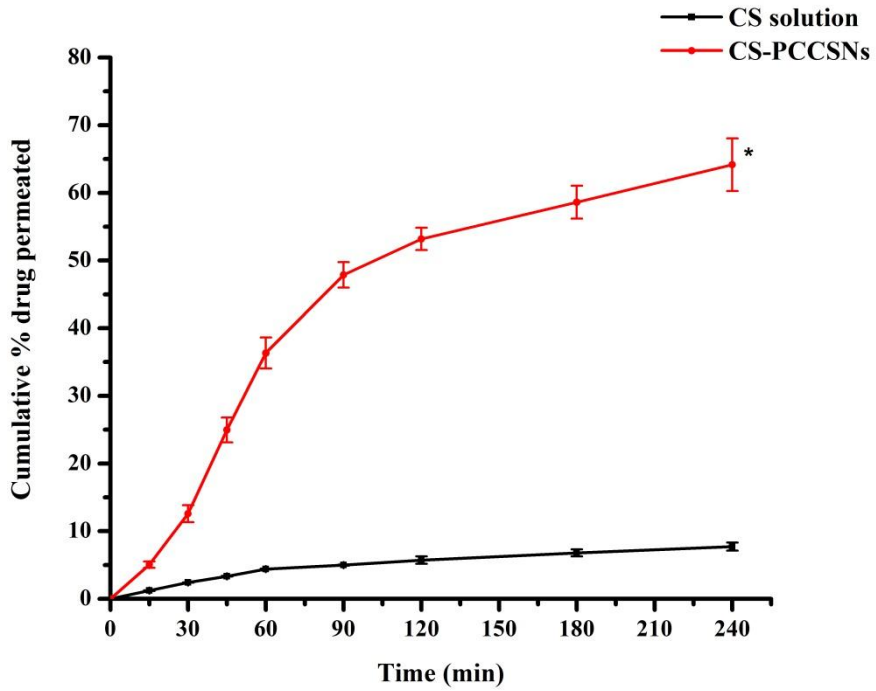

Figure 8.15 *Ex-vivo* permeation study of CS-PCCSNs and CS solution across rat intestinal membrane. Vertical bars represent ± SD; n=3; *significant at $p<0.05$ compared with CS solution (Unpaired student t-test)

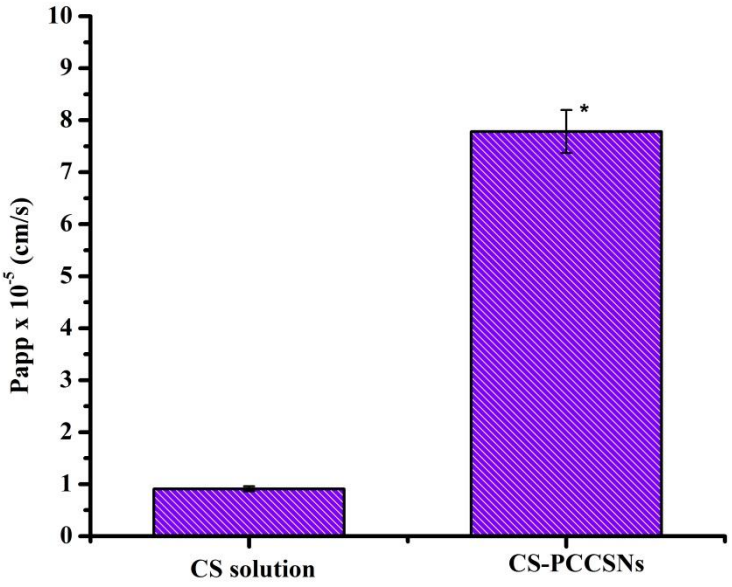

Figure 8.16 Apparent permeability coefficients (Papp) for CS from CS-PCCSNs and CS solution. Vertical bars represent ± SD; n=3, *significant at p<0.05 compared with CS solution (Unpaired student t-test)

The significant improvement (p<0.05) in the permeation of CS was observed in the form of CS-PCCSNs vis-à-vis CS solution across the rat intestine at each time point (Table 8.13). The permeability enhancement ratio for CS was found to be 8.55 $\pm$ 0.82 by developing CS-PCCSNs (Figure 8.16). The higher magnitudes of permeation for CS-PCCSNs construed that the large surface area furnished by their nanosized structure would have facilitated to get absorb through M cells of PP and transcellular as well as paracellular pathway across the intestinal enterocytes [106, 107]. Secondly, manipulation of the intercellular tight junction between the enterocytes by means of outer chitosan shell of CS-PCCSNs would also be the plausible cause for enhanced biopharmaceutical performance of the CS. Further, the enhanced residence in the biological membrane through mucoadhesive nature of the CS-PCCSNs could be the

added advantage to attain higher permeation and thereby, higher CS concentration in basolateral side [45, 232, 257, 258].

8.2.3.6 *In-vivo* intestinal uptake study

The *in-vivo* intestinal permeation potential of the CS-PCCSNs was visualized using confocal microscopy after oral administration in the rats. FITC tagged CS-PCCSNs were administered orally to the overnight fasted rats. The confocal microscopic images of the cross sections of rat intestinal tissue, showing the absorption of FITC tagged CS-PCCSNs are displayed in Figure 8.17. After 2 hr of oral administration of FITC tagged CS-PCCSNs, they were appeared throughout the intestinal tissue, including villi as well as follicle-associated epithelium as evinced by uniform, strong green colored fluorescence. The various stages of deep internalization of CS-PCCSNs, specifically mucosal and sub-mucosal (blood and lymphatic vessels) regions confirmed the progression of endocytosis inside the enterocytes, indicative of a true absorption [45]. The permeation was likely being due to endocytosis through M-cells of PP as well as transport through paracellular and transcellular route in the enterocytes [23, 49, 106, 196]. The luminance appeared on the apical surface of the villi construed the strong interaction between the cationic chitosan envelop and anionic aqueous mucous layer as well as cellular linings of the intestine, which would have bestowed the mucoadhesivity to CS-PCCSNs and thereby, prolonged the residence time in the mucosal membrane [234, 250, 258, 259]. As CS remains encapsulated within the CS-PCCSNs during the internalization process across GIT, it resulted in enhanced permeation, which further strengthens our hypothesis and the finding of *ex-vivo* studies. Hence, CS-PCCSNs could be a highly efficient transmucosal carrier for facilitating CS permeation across the intestinal barrier [196].

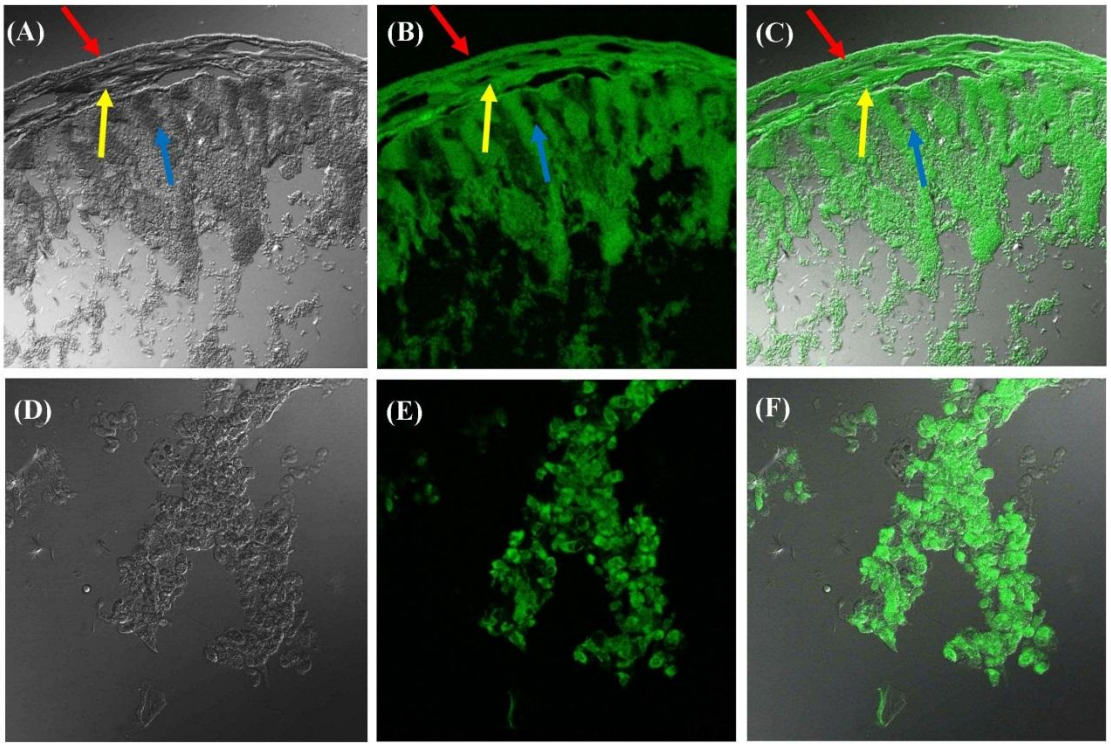

Figure 8.17 Confocal laser scanning micrographs of rat intestine, showing uptake and transport of FITC tagged CS-PCCSNs into the tissues, underlying the absorptive cells, after 2 hr of oral administration. (A) DIC image; (B) Fluorescent image; and (C) Merge of fluorescent and DIC image scanned at 10× plain. (D) DIC image; (E) Fluorescent image; and (F) Merge of fluorescent and DIC image scanned at 40× plain using emersion oil objective. Blue, yellow and red arrows indicate the mucosal, submucosal, and muscular regions of rat intestine, respectively in transverse section

8.2.3.7 *In-vivo* pharmacokinetic study

The plasma drug concentration-time profiles obtained after the single dose oral administrations of the CS solution and CS-PCCSNs in rats (20 mg/kg) are presented in Figure 8.18 and Table 8.14. The corresponding various pharmacokinetic parameters are summarized in Table 8.15. The total plasma concentration of CS was significantly increased (p<0.05) at each time point, by delivering the CS in the form of CS-PCCSNs as compared to that of CS solution. Non-compartmental (model

independent) analysis of CS plasma concentration time profile exhibited marked superiority in the pharmacokinetic parameters for CS-PCCSNs vis-à-vis the CS solution. As can be seen from the plasma drug concentration–time curve, oral administration of CS solution resulted into faster appearance of CS in blood. The C_{max} of 349.42 ± 11.21 ng/ml was observed for CS-PCCSNs after single dose administration, which was ~3.1 times higher than those obtained for the CS solution (112.23 ± 5.90 ng/ml). This might be ascribed to their specialized absorption mechanisms across the GIT conceivably as a consequence of their nano-sized structure and surface properties [27, 226].

Table 8.14 Plasma drug concentration time profile data of CS solution and CS-PCCSNs following single dose oral administration in rats

Time (hr)	Plasma concentration of CS (ng/ml)	
	CS solution	**CS-PCCSNs**
0	0	0
0.25	11.42 ± 1.36	9.72 ± 1.74
0.5	50.59 ± 4.30	40.06 ± 2.62
1	112.23 ± 5.90	82.21 ± 4.56
2	70.08 ± 2.86	183.16 ± 7.89
4	28.75 ± 2.10	349.42 ± 11.21
8	ND	259.83 ± 7.82
12	ND	151.49 ± 3.46
24	ND	71.87 ± 4.54
48	ND	9.08 ± 3.68

All values reported are mean ± SEM, (n=6); ND: Not detected

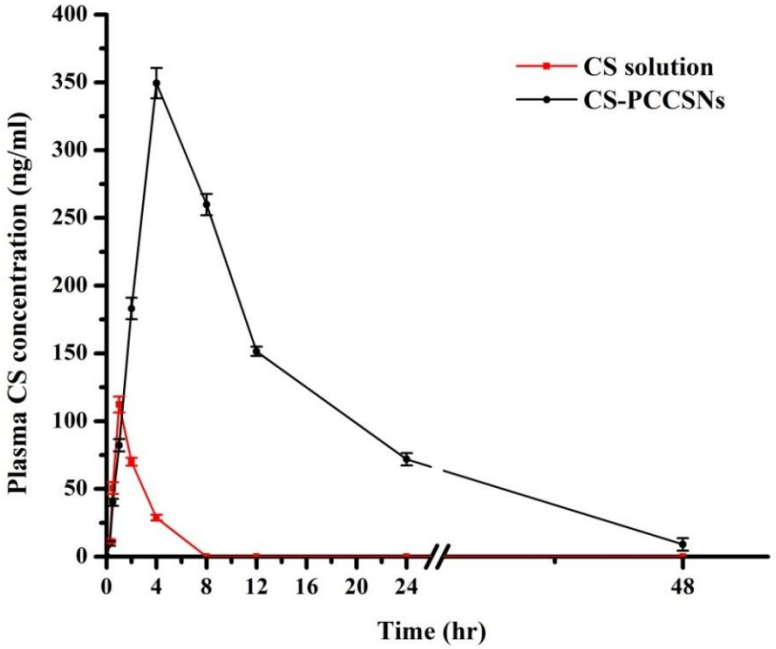

Figure 8.18 Plasma drug concentration time profile of CS-PCCSNs and CS solution following single dose oral administration in rats; Dose: 20 mg/kg (vertical bars represent ± SEM; n=6)

The T_{max}, $T_{1/2}$ and MRT obtained with CS-PCCSNs were significantly higher than those obtained with pure CS solution. The T_{max} showed drastic delay up to 4 fold for CS-PCCSNs over the CS solution, confirming the sustained *in-vivo* CS release potential of CS-PCCSNs [106, 107, 235]. This was because of chitosan shell, which would have confined the CS release by imparting the diffusional barrier. Further, it might be also due to uptake by M cells of PP, which would have transported the CS-PCCSNs to the systemic circulation through lymphatic vessels and thus, taken longer time as compared to other routes [67, 249]. Besides, significant improvement (p<0.05) in $T_{1/2}$ and MRT was noticed for CS-PCCSNs than those obtained for free CS solution, suggesting the prolongation of blood circulation time of CS-PCCSNs along with slower release, which might be due to the hydrophilic chitosan shell.

Moreover, longer retention of CS-PCCSNs in an intestinal mucosa also might be one of the reasons for longer MRT [67, 107, 258].

Table 8.15 Pharmacokinetic parameters of CS and CS-PCCSNs following single oral administration in rats (Dose: 20 mg/kg)

Parameters	CS solution	CS-PCCSNs
C_{max} (ng.ml^{-1})	112.23 ± 5.90	349.42 ± 11.21*
T_{max} (hr)	1 (± 0)	4 (± 0)
$AUC_{0\text{-}48h}$ (ng.hr.ml^{-1})	232.16 ± 12.31	4556.94 ± 320.91*
$AUC_{0\text{-}\infty}$ (ng.hr.ml^{-1})	295.53 ± 17.79	4978.65 ± 211.40*
$T_{1/2}$ (hr)	1.52 ± 0.02	9.74 ± 0.56*
MRT (hr)	2.79 ± 0.03	15.34 ± 0.50*
Fr	1	19.75 ± 1.74*

**significant values at p<0.05 compared with CS solution (Unpaired student t-test); All values reported are mean ± SEM, (n=6).*

Likewise, significantly improved (p<0.05) $AUC_{0\text{-}48hr}$ and $AUC_{0\text{-}\infty}$ were noticed for CS-PCCSNs over the pure CS solution, ratifying the potential of CS-PCCSNs with improved rate and extent of oral drug absorption. From the various pharmacokinetic parameters, it was clear that CS-PCCSNs have the promising potential for oral delivery of CS with approximately ~19.75 fold higher relative bioavailability, compared to pure CS solution, upon single dose oral administration. The significant improvement (p<0.05) in the oral bioavailability of CS, achieved with CS-PCCSNs was due to superior encapsulation of CS inside the PCCSNs, which would have facilitated their absorption through various routes i.e., M cells of PP as well as trancellular and paracellular pathway across the enterocytes of GIT [23, 106, 107, 236]. Additionally, chitosan envelop would have also improved the permeation of CS-

PCCSNs by structural reorganization of tight junction associated proteins, with the aid of ionic interactions in order to facilitate the paracellular transport [232, 258, 259]. Results corroborate well with the findings of *ex-vivo* and *in-vivo* intestinal permeation studies and further substantiate the hypothesis.

8.2.3.8 *In-vivo* mast cell stabilizing activity

The results of mast cell stabilizing activity of CS-PCCSNs in the rats are summarized in the Table 8.16. The degradation of the isolated peritoneal mast cells in different groups, after incubation with the compound 48/80 is depicted in Figure 8.19. In the normal control group, isolated peritoneal mast cells showed 10.515 ± 0.8813 % activation. Whereas, positive control group showed 93.033 ± 3.648 % activation of mast cells, upon incubation with compound 48/80. Prophylactic treatment with oral administration of the CS solution (20 mg/kg) and CS-PCCSNs (20 mg/kg on 1^{st}, 3^{rd}, 5^{th} and 7^{th} day) for 7 days in the rats has offered significantly higher ($p<0.05$) protection against mast cell degranulation and reduced the total number of activated mast cell. Oral administration of CS solution provided ~10.87 % protection against mast cell degranulation compared to positive control and showed 82.92 ± 1.558 % activation after incubation with compound 48/80. However, significantly much higher protection against mast cell degranulation was observed in case of CS-PCCSNs as compared to CS solution ($p<0.001$).

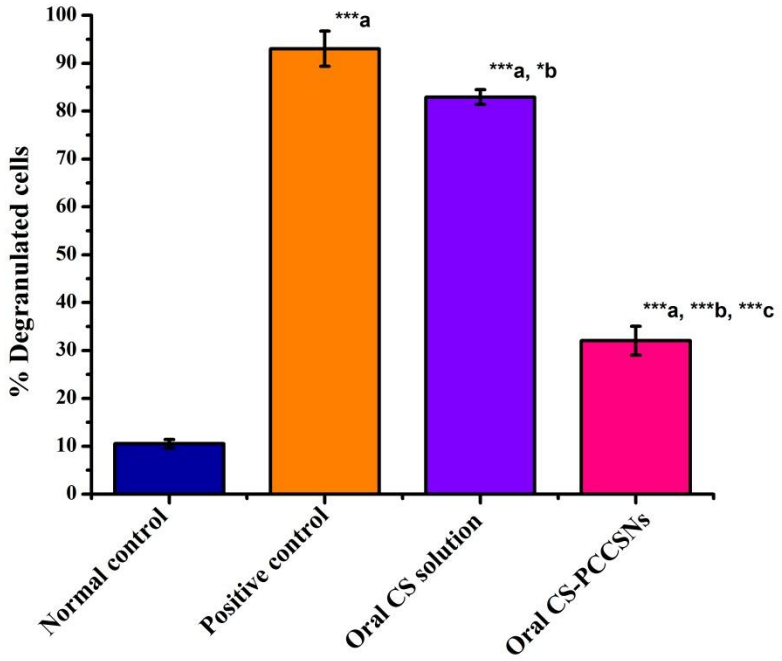

Figure 8.19 Effect of oral administration of CS solution and CS-PCCSNs on degranulation of peritoneal mast cells in rats (Dose: 20 mg/kg); Vertical bars represent ± SEM; n=6.

******p*<0.001, **p*<0.05; a *vs* normal control, b *vs* positive control and c *vs* oral CS solution; One-way ANOVA followed by Tukey's multiple comparison test**

Oral administration of CS-PCCSNs provided ~65.53 % protection against mast cell degranulation compared to positive control and showed 32.065 ± 3.014 % activation after incubation with compound 48/80. Additionally, lower amount of histamine release for CS-PCCSNs treated group compared to CS solution treated and positive control group suggested the better efficacy of CS-PCCSNs for stabilizing the mast cells from compound 48/80 like allergen evoked degranulation [199-202].

Table 8.16 Effect of oral administration of CS solution and CS-PCCSNs on compound 48/80 induced degranulation of peritoneal mast cells and histamine release in rats (Dose: 20 mg/kg)

Treatment Groups	% degranulated cells	Histamine release (µg/ml)
Normal Control	10.515 ± 0.881	0.033 ± 0.0019
Positive Control	93.033 ± 3.648***[a]	0.190 ± 0.0083***[a]
Oral CS solution	82.920 ± 1.558***[a,*b]	0.166 ± 0.0043***[a,*b]
Oral CS-PCCSNs	32.065 ± 3.014***[a,***b,***c]	0.065 ± 0.0068**[a,***b,***c]

*All values reported are mean ± SEM, (n=6). ***p<0.001, *p<0.01, *p<0.05; a vs normal control, b vs positive control and c vs oral CS solution; One-way ANOVA followed by Tukey's multiple comparison test.*

The enhanced efficacy for CS-PCCSNs compared to CS solution after oral administration indicated that CS-PCCSNs would have delivered significantly higher amount of CS in the systemic circulation by improving its GIT permeability compared to CS solution and thereby, provided higher protection to the sensitized mast cells against degranulation, which in turn strengthens the findings of *in-vivo* pharmacokinetic study. Moreover, highest protection against mast cell degranulation compared to other developed systems (i.e., CS-PNs, CS-SLNs, CS-PLHNs), confirming the superiority of CS-PCCSNs as an oral transmucosal delivery system compared to other developed systems.

8.3 Summary

The present strategy provides a deep insight into the captivating aspects of PCCSNs for oral delivery of CS like poorly permeable hydrophilic drug molecule. The CS-PCCSNs were successfully formulated by modified nano-coprecipitation method. The

Plackett-Burman screening design was used for preliminary screening of large number of process as well as formulation variables in order to identify critical variables affecting the formulation characteristics of CS-PCCSNs. A 3-level, 3-factor Box-Behnken experimental design was imperatively enforced to optimize and to understand the combined influence of screened critical variables (i.e., concentration of PCL, concentration of chitosan and concentration of surfactant) on physicochemical properties of CS-PCCSNs, i.e., particle size, EE and PDI. The quality by design approach suggested that Box-Behnken experimental design provided a high degree of prediction and realization for optimization of the physicochemical properties of CS-PCCSNs by controlling the different formulation variables. The formulation was optimized by employing numerical optimization based desirability technique in order to obtain CS-PCCSNs with maximum EE and minimum particle size having narrow particle size distribution. The successfully optimized CS-PCCSNs showed particle size of 194.2 $\pm$ 4.3 nm, EE of 77.34 $\pm$ 1.1 % and PDI of 0.130 $\pm$ 0.026. The optimized batch has desirability of 0.628. The solid state characterizations of optimized CS-PCCSNs suggested the encapsulation of CS in an amorphous form inside the matrix of PCCSNs without any physical as well as chemical interactions. The morphological studies pointed towards the existence of smooth, spherical shaped, core-shell architecture of CS-PCCSNs. *In-vitro* release study of CS-PCCSNs in phosphate buffer pH 7.4 showed extended release up to 48 hr by diffusion controlled process. The optimized CS-PCCSNs were stable with respect to their physicochemical attributes, stored at different environmental conditions over the period of 6 months. *Ex-vivo* intestinal permeation study demonstrated ~8.55 fold improvements in CS permeation across the intestinal barrier by forming CS-PCCSNs as compared to pure CS solution. Further, *in-vivo* intestinal uptake study performed using confocal

microscopy following oral administration confirmed the permeation potential of CS-PCCSNs, as indicated by their strong green colored fluorescence. *In-vivo* single dose oral bioavailability study was performed in rats and revealed ~19.75 fold enhancements in oral bioavailability of CS after its incorporation into PCCSNs as compared to pure CS solution, which ought to be nano-sized structure of PCCSNs as well as permeation enhancing effect of the cationic, chitosan shell of PCCSNs. Eventually, *in-vivo* mast cell stabilizing activity performed in rats demonstrated significant protection against mast cell degranulation with oral administration of CS-PCCSNs than free CS solution. Conclusively, the developed CS-PCCSNs could definitely be considered as promising delivery approach for altering the existing marketed formulations of CS as a result of its improved oral bioavailability with greater efficacy.